AD-A228 119

JHU-CNDE-IW-7

(2)

Characterization of Elastic Properties of Interfaces in Composite Materials

T.M. Hsieh, K.A. Hirshman, E.A. Lindgren, M. Rosen

September 1990

Final Report

Contract N00014-87-K-0341

for

Steven G. Fishman, Program Manager
Department of the Navy
Office of Naval Research
Arlington, VA 22217

Table of Contents

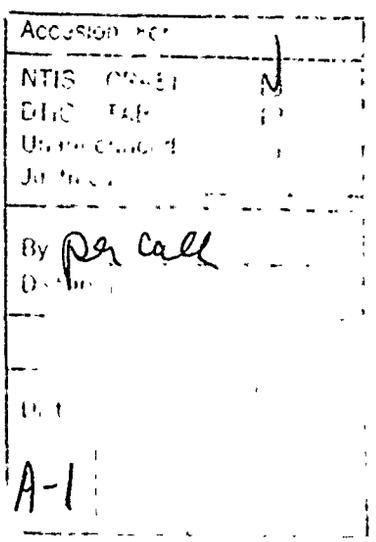

I. Executive Summary

The Strategic Defense Initiative Organization has placed a great deal of emphasis on the development of new composite materials, specifically metal and ceramic matrix composites. These types of composite materials offer the advantages of being lighter, stiffer, stronger, and more resistant to creep and corrosion. However, because of the physical and chemical differences of the matrix and reinforcing agents the interface is plagued by chemical reactions and a high level of residual stress. This impedes the ability of the interface to bear and transfer load and results in fracture upon subsequent loading. Thus, the need for nondestructive characterization of interfaces is critical to the development of these high technology composite materials.

Feedback from a nondestructive interface characterization technique is also critical to the further development and refinement of the materials processing procedures. The unique propagation characteristics of leaky interface waves appear to be ideally suited for this purpose. While bulk moduli measurements usually yield relatively poor average values of modulus for fiber reinforced composites, leaky waves offer the potential for microscopic measurement of these physical parameters at localized regions of interest. It is clear that nondestructive interface characterization is necessary for the accurate modeling of the mechanical behavior of metal matrix composites. Interface wave propagation measurements may provide the necessary information for modeling the micro and macrobehavior of these composites.

The goal of the Johns Hopkins University program was to study these characteristics and develop techniques which utilize interface waves for nondestructive evaluation of composite interfaces. This final report summarizes the results of two projects which examined the use of interface waves for nondestructive evaluation of interfaces. The first project focused on Stoneley waves and their sensitivity to interfacial bond quality and microstructural changes. The results demonstrated that Stoneley waves propagate with higher velocities through interfaces of good surface finish than they do through interfaces comprised of poorly finished surfaces. Stoneley interface wave velocities were also found to be dependent on the quality of the bond and the microstructure at the interface.

The second project focused on the use of leaky waves for the nondestructive characterization of interfaces. Remote generation of leaky waves along a planar silicon carbide/aluminum interface was demonstrated by mode conversion of a longitudinal wave incident at an angle equivalent to the leakage angle. Direct measurement of interface wave leakage was also accomplished. It was shown that remote generation of leaky

waves and direct measurement of interface wave leakage in a silicon carbide/aluminum interface is a viable method for nondestructive evaluation and characterization of a planar interface.

The results achieved during this program are summarized below:

- Stoneley interface waves were generated and detected between steel-titanium planar interfaces. It was shown that Stoneley waves are sensitive to changes in microstructure near the bondline.

- Stoneley waves were shown to be sensitive to the amount of bonding between two surfaces.

- Development of an approach to launch leaky modes by conversion from a bulk wave incident on a bonded interface at a critical angle was accomplished. It was shown that remote generation is a valuable method for exciting leaky modes when direct access to the interface is impossible.

- Experimental verification of several of the theoretically predicted interface modes for a planar silicon carbide/aluminum interface.

- Remote measurement of the leakage energy of an interface wave was accomplished. It was concluded that this direct measurement of leakage is a valuable method for separating modes and will contribute to nondestructive interface characterization.

- It was shown that leaky waves offer several potential benefits for nondestructive interface wave characterization including detection of disbonds and elastic characterization.

This program demonstrated the feasibility of guided interface wave techniques for determining the elastic properties and adhesion of interfaces. In order to achieve the goal of a simple and accurate nondestructive method for composite interface characterization, further work must be done to implement the techniques developed here for use on actual composite materials.

II. Introduction

The advantages offered by metal and ceramic matrix composites for structural aerospace applications is evident by the widespread use of these new materials. However the mechanical properties and structural integrity of these composites are largely determined by the elastic, anelastic and plastic behavior of the interface between the matrix and reinforcing agent. Feedback from a nondestructive interface characterization technique is critical to the further development and refinement of the processing procedures for these materials. No method exists for the determination of the local elastic properties at composite interfaces. The purpose of the Johns Hopkins University program is to develop such a technique to characterize interface properties and to use it to study to micromechanics of composites. This will also provide an opportunity to understand the relationship between process variables and interface properties.

References to the existence of acoustic waves that travel along an interface have sporadically appeared in the literature since they were first predicted by Richard Stoneley in 1924. Many of these presented theoretical predictions of wave propagation between two ideal media with only a few papers citing experimental observations. Interface waves are defined as elastic waves which propagate along the boundary between two solid half-spaces with both longitudinal and shear components of particle motion. It has been shown that they are sensitive to near bond line conditions including microstructural variations and degree of contact. Recently, renewed interest in these types of waves has developed because of their potential applications for characterizing composite interfaces.

The scientific research goal of The Johns Hopkins University program is to develop a nondestructive technique to characterize the properties of interfaces. The specific goals of the research agenda include the following:

- Study the propagation characteristic of ultrasonic Stoneley and leaky waves and their sensitivity to interfacial bond quality and microstructural variations.

- Develop techniques for the generation and detection of leaky waves at a composite interface.

- Evaluate the potential of these waves for nondestructive evaluation of local elastic properties at interfaces.

III. Background

Interface waves are elastic waves which propagate along the plane boundary between two different elastic solid media. They are, generally, classified in two groups by energy flow characteristics. The energy of leaky waves is attenuated as it propagates along the boundary region with both normal and parallel components of particle displacements. Energy is radiated away from the interface into the less dense material, hence the name leaky waves. Stoneley waves are non-leaking waves that propagate unattenuated along the interface if the materials at the boundary satisfy certain requirements. The bulk of the research that has appeared in the literature has concentrated on Stoneley waves and has been analytical in nature. Very few of these have presented experimental observations of interface waves of either type.

By considering the energy dissipation of seismic disturbances, Richard Stoneley [1] first predicted the existence of these waves in 1924. He postulated that they are similar in nature to Rayleigh and Love waves, but propagate between adjacent layers of subterranean rock. Essentially, Stoneley extended Lord Rayleigh's earlier work on surface waves by modeling the interface as the plane boundary between two isotropic elastic half spaces [2,3,4]. Both continuity of stress and particle displacement across the boundary was assumed. The characteristic Stoneley equation shown in Figure 1 has 8 roots for the complex velocity V^2. Therefore, there are 16 possible values of V, 8 of which are independent. To interpret this equation, Stoneley resorted to the case where the longitudinal and shear waves were approximately equal for an incompressible media, although the densities were assumed to be different. Under these conditions, a positive real root was found always to exist for the quantity V_{St}/V_S, where V_{St} is the Stoneley wave velocity and V_S is the shear wave velocity. The root was always less than unity indicating that the velocity of the Stoneley wave was less than that of the shear wave. It was concluded that these types of waves may only exist if the densities and Lame's constants approximately satisfy Weichert's condition which states, $\rho_1/\rho_2 = \lambda_1/\lambda_2 = \mu_1/\mu_2$, where λ and μ are Lame's constants, ρ is the density, and the subscripts denote the two solids.

Sezawa and Kanai [5,6,7] re-derived the Stoneley equation and analytically determined that in certain situations a longitudinal or normally polarized shear wave incident at an oblique angle upon a solid-solid interface would have interface, as well as reflected and refracted wave components. They also investigated the possible range of existence for these types of waves in terms of the densities and Lame's constants. It

was ascertained that for a large ratio of the densities $\rho_1/\rho_2 > 2$ or a small ratio $\rho_1/\rho_2 < 0.5$, the range of μ_1/μ_2 for Stoneley wave existence is relatively wide. When the ratio of the densities is near unity, Stoneley waves cannot exist unless Weichert's condition is satisfied. Further analysis showed that Stoneley waves, like Rayleigh waves, are non-dispersive. Scholte [8,9] extended the calculations of Sezawa and Kanai and examined the existence range for Stoneley waves for several pairs of theoretical material pairs.

Velocity, amplitude, and particle motion of these waves was studied through mathematical analysis by Yamaguchi and Sato [10]. They determined that the lower limit of Stoneley wave velocity is the Rayleigh wave velocity which is given as $(0.8453...)^{1/2}V_S$. The ratio of the amplitude of the vertical component (w) and of the horizontal component (u) was found to be a minimum when $(V_{ST}/V_S)^2 = 0.8453...$ This corresponds to a situation analogous to a Rayleigh wave. As the ratio of the displacements increases, the ratio of the densities increases. However, as ρ_1 approaches ρ_2 the horizontal component begins to shrink. When the two densities are equal, the horizontal component disappears. By analyzing the expressions that represent the real components of displacement, it was also shown that the rotation of the particle orbit was in an elliptical retrograde type motion similar to that of a Rayleigh wave.

Several papers have appeared in the literature which have shown results of calculations of Stoneley wave velocities. Ginzbarg and Strick [11] graphically presented ratios of Stoneley wave velocities and shear wave velocities for a wide range of elastic properties. Owen [12] showed that of 900 isotropic materials, only 30 pairs would support Stoneley waves.

Stoneley waves in anisotropic materials was examined by Lim and Musgrave [13]. Calculations for an interface composed of two crystalline half-spaces of cubic symmetry revealed that there are several orientations which would allow the propagation of an interface wave. It was also shown that the amplitude of these waves dampen in a sinusoidal fashion with increasing distance from the source instead of in an exponential manner as seen in isotropic materials. Chadwick and Currie [14] were able to demonstrate that the secular equation for interface waves can be constructed directly from the complex vectors that result from the analysis of Rayleigh waves on a free surface. This equation was then reduced to a single real relation to demonstrate that Stoneley waves in anisotropic materials are not restricted to certain directions of propagation, but that the wave speed continuously depends on the parameters of the transmitting materials.

$$
\begin{vmatrix}
2\rho_1 V_{S1}^2\sqrt{\left[1-\left[\frac{V_{ST}}{V_{L1}}\right]^2\right]} & 2\rho_2 V_{S2}^2\sqrt{\left[1-\left[\frac{V_{ST}}{V_{L2}}\right]^2\right]} & 2\rho_1 V_{S1}^2\sqrt{\left[2-\left[\frac{V_{ST}}{V_{S1}}\right]^2\right]} & 2\rho_2 V_{S2}^2\sqrt{\left[2-\left[\frac{V_{ST}}{V_{S2}}\right]^2\right]} \\
\rho_1\left[V_{ST}^2 - 2V_{S1}^2\right] & -\rho_2\left[V_{ST}^2 - 2V_{S2}^2\right] & -2\rho_1 V_{S1}^2\sqrt{\left[1-\left[\frac{V_{ST}}{V_{S1}}\right]^2\right]} & 2\rho_2 V_{S2}^2\sqrt{\left[1-\left[\frac{V_{ST}}{V_{S2}}\right]^2\right]} \\
1 & -1 & \sqrt{\left[1-\left[\frac{V_{ST}}{V_{S1}}\right]^2\right]} & -\sqrt{\left[1-\left[\frac{V_{ST}}{V_{S2}}\right]^2\right]} \\
\sqrt{\left[1-\left[\frac{V_{ST}}{V_{L1}}\right]^2\right]} & \sqrt{\left[1-\left[\frac{V_{ST}}{V_{L2}}\right]^2\right]} & 1 & 1
\end{vmatrix} = 0
$$

Figure 1. Determinantal boundary equation for Stoneley interface waves where ρ is the density VST the Stoneley wave velocity, V_L the longitudinal wave velocity, V_S the shear wave velocity, and the subscripts refer to two different media.

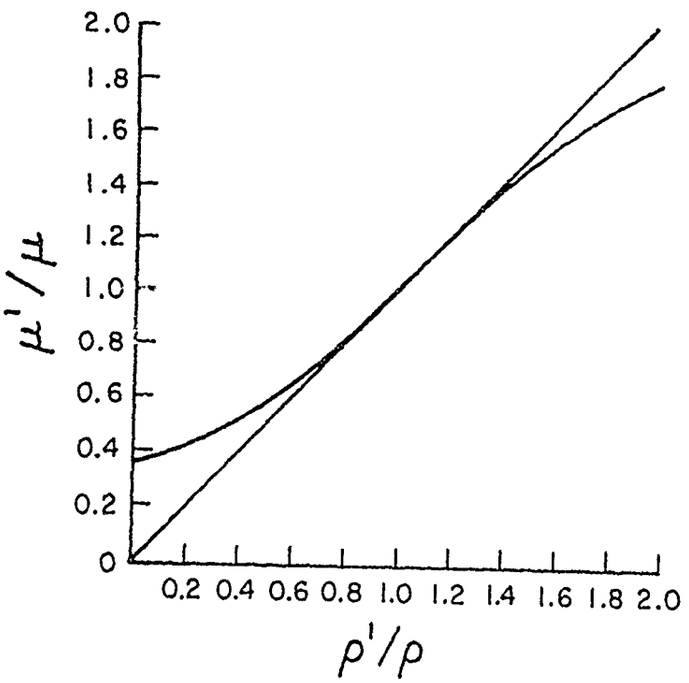

Figure 2. Possible range of existence of Stoneley waves for $\lambda = \mu$, $\lambda' = \mu'$ between curves from Sezawa and Kanai [5].

The sixteen independent roots of the Stoneley wave equation were studied in-depth by Pilant [15]. By varying the material parameters over a wide range, the behavior of the sixteen roots was examined. His mathematical analysis showed that there are two types of behavior outside the range of existence of Stoneley waves. First, an attenuated leaky wave will propagate if the denser material has a faster velocity than the less dense material. If the difference in velocity is greater than about a factor of three, the leaky root disappears and the energy is propagated as a Rayleigh-type wave. The second case involves a less dense material with an acoustic velocity much faster than the more dense material. Although this case is of little physical significance, it is interesting that the results of the analysis predict that no energy would propagate.

The studies mentioned above dealt with interface waves in a purely analytical nature. One of the earliest reported experimental observations of interface waves was in 1977 by Lee and Corbly [16]. Utilizing a mode conversion technique, they were able to generate and detect Stoneley and leaky waves on both planar and cylindrical geometries. Interface waves were generated by mode conversion from Rayleigh waves between Al/Ti, steel/Al, and Ti/steel pairs. In the planar case, each couple was composed of a larger base plate and a smaller plate which rested on top. A schematic diagram of their experimental set-up is shown in Figure 3. A Rayleigh wave which was generated on the surface of the base plate mode converted to an interface wave at the boundary. This interface wave propagated along the boundary region until it re-converted to a Rayleigh wave at the far side of the top plate. Travel times were measured as a function of stress applied to the couple. Figure 4 shows an ultrasonic echo wave train from a steel/aluminum specimen. The generally good quantitative agreement found between the predicted interface wave velocity and the measured wave velocities suggested the possibility of utilizing these wave for nondestructive inspection of joints coupled by interference-fit fasteners.

A direct optical measurement of interface waves was reported by Claus and Palmer [17,18,19,20] in which the normal component of wave motion was observed between a nickel/pyrex couple. Utilizing a differential interferometric optical system, they were able to measure the normal component of interface wave propagation and attenuation as a function of surface roughness. A scan of the interface wave is shown in Figure 5. The interface waves were generated by mode conversion from Rayleigh waves between several pairs of materials which were held together by mechanical compression and adhesive bonding. Their results also suggested potential applications for nondestructive evaluation of adhesively bonded materials.

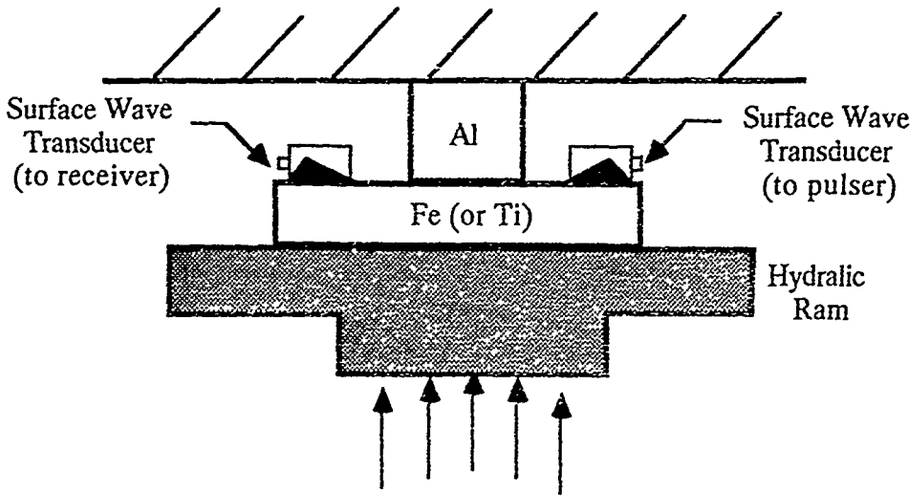

Figure 3. Schematic representation of the experimental set-up used by Lee and Corbly to measure Stoneley wave on a planar interface.

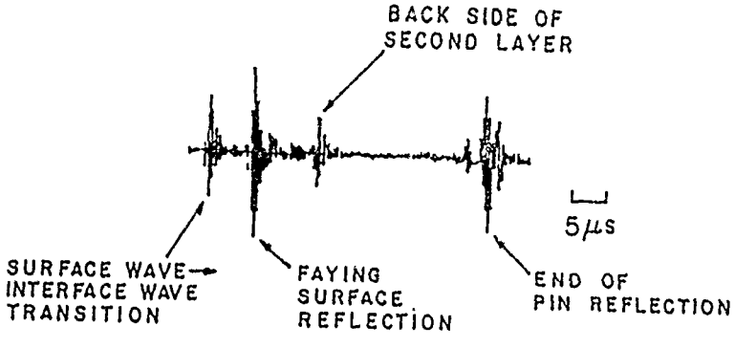

Figure 4. Ultrasonic echo wave train from a steel/aluminum specimen from Lee and Corbly [16].

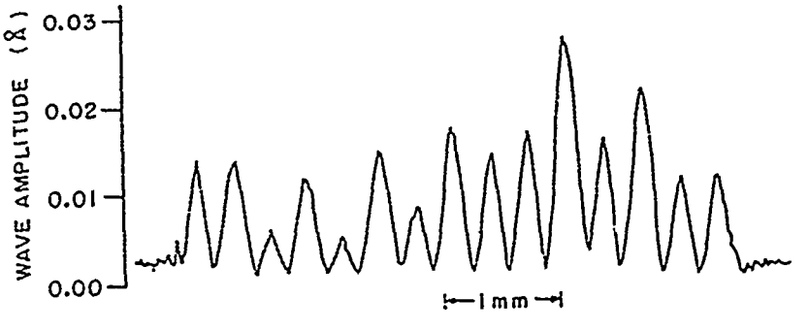

Figure 5. Scan of Stoneley wave on the interface between clamped Corning 7070 Pyrex and nickel samples from Claus and Palmer [17].

IV. Experimental Considerations

IV.1 Physical Characteristics of Interface Waves

Interface wave is a generalized term used to describe two dissimilar but related types of waves that travel along the plane boundary between two different solid materials. From the analytical results presented by some of the papers mentioned in the previous section, the important physical characteristics of Stoneley and leaky waves may be summarized.

Stoneley waves correspond to real solutions of the wave equation (Figure 1). This implies that they exist only for a limited range of material pairs including steel/titanium and nickel/pyrex. The existence criterion has been simplified to satisfaction of Weichert's condition for isotropic materials or in more general terms that the shear wave velocities of the two materials be nearly equal. The velocity of the Stoneley wave is highly dependent on the Poisson's ratio of the denser material, while

the Poisson's ratio of the less dense material has little influence. It is bounded at the lower end by the fastest Rayleigh velocity and at the upper end by the slowest shear velocity. These waves travel along the interface with the wave energy confined to a region near the boundary. None of the energy is radiated away from the interface. Particle displacement is composed of normal and parallel components which are attenuated with distance into either medium. These displacements have been described as elliptical retrograde in the denser material similar to that of a Rayleigh wave. A schematic diagram of this motion is shown in Figure 6.

Leaky interface waves correspond to the complex solution of the wave equation. This suggests that leaky waves will exist for many more material pairs, since the existence criterion is not as stringent. It is possible for a leaky wave to exist if the wave velocity of the denser material is greater than the wave velocity of the less dense material. The particle motion of these waves is also elliptical retrograde in the denser medium, but resemble shallow shear wave fields in the less dense medium. Part of the wave energy is radiated away from the interface into one or both of the bounding materials at an angle proportional to the imaginary component of the solution to the wave equation. Figure 7 depicts this motion. For a detailed mathematical analysis of the sixteen roots see Pilant [11].

V. Stonely Wave Propagation for NDE

V.1 Introduction

This investigation focused on the sensitivity of Stoneley interface waves to interfacial bond quality, and their ability to evaluate microstructural change. Through various heat treatments of 4340 steel, several pearlitic and martensitic microstructures were obtained. The steel samples were each coupled with a Titanium-6 Aluminum-4 Vanadium sample, and Stoneley interface waves were generated along the planar interface between the two specimens. The Stoneley interface waves were generated and detected by Rayleigh mode conversion wedges. The corresponding ultrasonic velocities were calculated using time-of-flight measurements as a function of microstructure, surface finish, and interfacial bond quality.

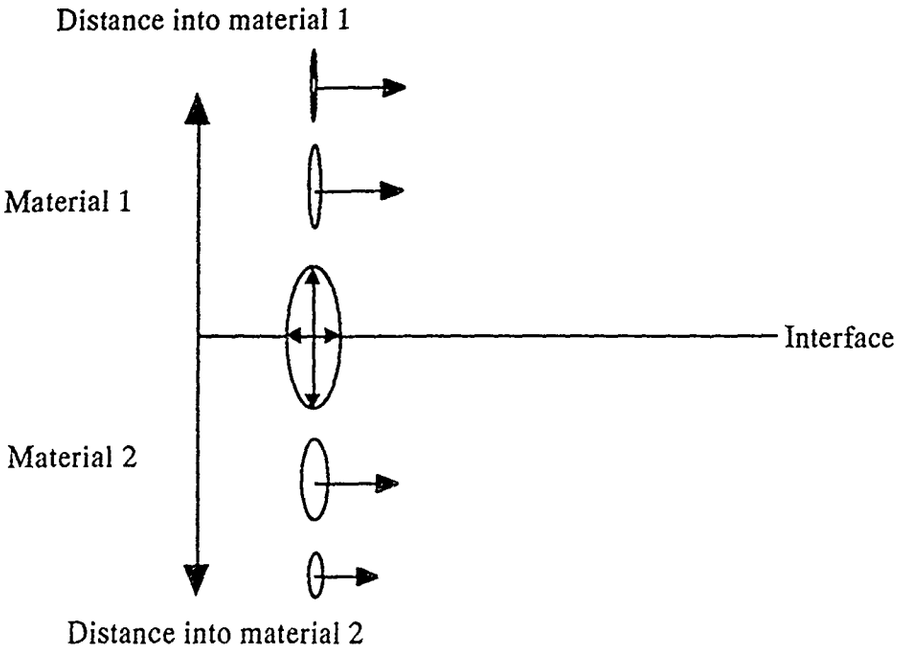

Figure 6. Schematic representation of the elliptical retrograde particle rotation of a Stoneley interface wave with both normal and parallel components. The constant ellipse size along the x-axis represents the fact that the energy of these waves is confined to a region near the interface are non-attenuative.

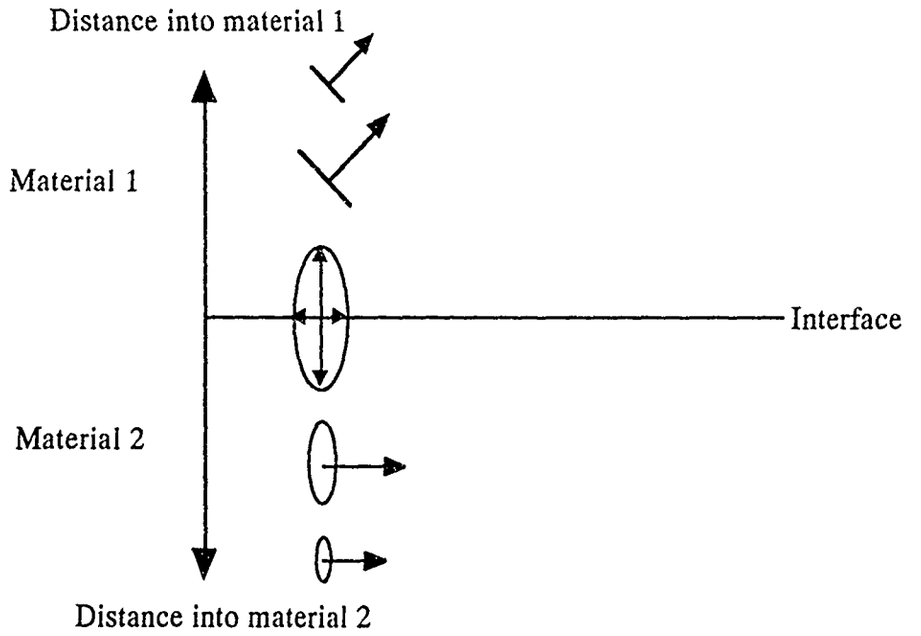

Figure 7. Schematic representation of the elliptical retrograde particle rotation of a leaky interface wave with both normal and parallel components. The decreasing size of the ellipses represents the fact that part of the energy is radiated away from the Interface into the less dense material.

V.2 Experimental Procedure

Five 4340 steel specimens were cut from a 305 cm x 5.08 cm x 1.27 cm slab. The lengths of the five specimens were varied between 18 and 23 centimeters for identification purposes. Five smaller pieces were also cut from the original plate to pair each one with a large specimen.

Heat Treatments

Heat treatments were performed on the five specimens to obtain five different microstructures. The Time-Temperature-Transformation (T-T-T) diagram for 4340 steel was used for heat treatment informational purposes (Figure 8) [21]. Specimen one was kept in its as-received state for comparison purposes. Specimen two was austenitized at 843°C for 90 minutes. It was then transferred to a molten salt heater at 648°C for approximately 48 hours to transform the microstructure to coarse pearlite (see transformation diagram). After isothermal cooling, it was allowed to air-cool to ambience. Specimen three was austenitized at 843°C for 70 minutes, quenched in oil for 6 minutes and then quenched in water until ambient temperatures were reached. The transformation diagram revealed the time period needed to obtain a fully quenched martensite is well within the period of time required to quench a 1.27 centimeter thick slab. The fourth specimen was austenitized at 843°C for 70 minutes and then quenched in oil for 6 minutes. The sample was then transferred to a liquid nitrogen bath for 10 minutes and allowed to reach ambient temperatures. The specimen was then tempered at 204°C for 100 minutes and then quenched in oil. The fifth specimen was austenitized at 843°C for 70 minutes and was air-cooled to room temperature or normalized.

Metallography

Sections approximately 1.27 cm x 0.635 cm x 0.635 cm were cut from all five smaller steel slabs. These five pieces were mounted into clear Lucite to provide a cross-section for metallography. The five specimens were mechanically sanded on 60 grit to 600 grit paper and then polished on three wheels: six micron diamond, three micron diamond, and one-half micron aluminum oxide. A nital etch, 2 ml. of HNO_3 and 98 ml. of ethanol, was applied to the steel specimens to prepare for microstructural observation. The titanium alloy was also prepared for metallographic observation. A block, 5.08 cm x 5.08 cm x 1.918 cm, was ground to have two large, flat, parallel faces. For metallographic purposes, one side was subjected to the same polishing process as the 4340 steel specimens. A Kroll's reagent, 1-3 ml. of HF, 2-6 ml. of HNO_3 and H_2O

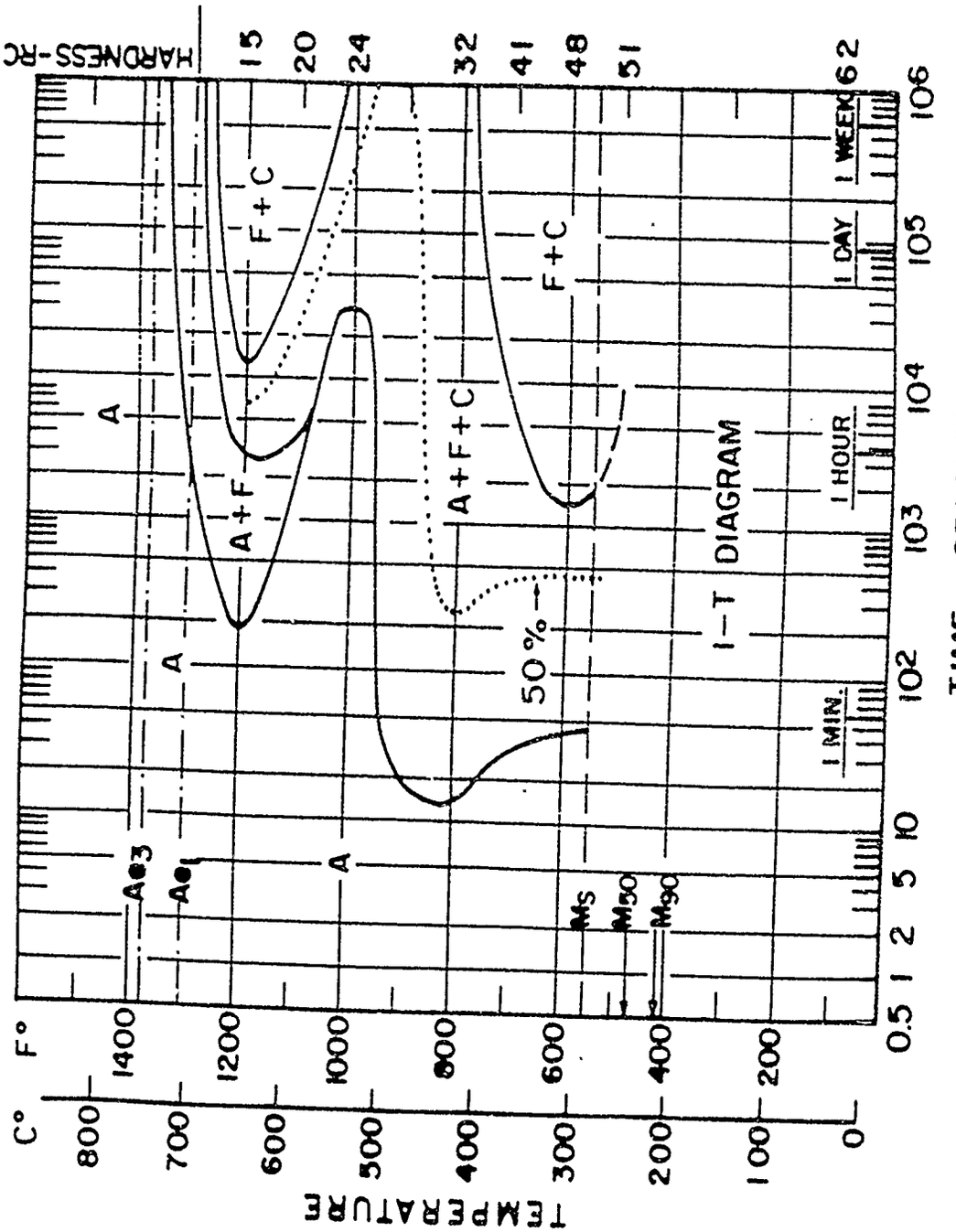

Figure 8. Time-Temperature-Transformation diagram for 4340 steel.

to 1000 ml., was applied to the surface and allowed to react for fifteen seconds to prepare for microstructural observation. Metallographic examination was performed on a Unitron inverted stage metallograph. The 4340 steel specimens were examined at magnifications of 160x, 320x, 500x, and 1000x to reveal the various microstructures completely. The titanium specimen was observed at 100x, 320x, 500x, and 1000x to examine the preferred orientation of the grains.

Hardness

Rockwell "B" hardness measurements were performed on specimens one and two. The hardness tester was calibrated using standard calibration test blocks to a value of plus or minus one Rockwell "B" hardness point. The measurements were performed on pieces cut from the smaller steel slabs. By traversing the specimens in three perpendicular directions, an average hardness value could be obtained. Rockwell "C" tests were performed on steel specimens three, four, five, and the titanium alloy. The hardness tester was again calibrated and measurements were performed across each specimen in three perpendicular directions.

Density Measurements

Density measurements were performed on the five steel samples and the titanium alloy by a method developed by Davis and Schoonover [22-23]. A high precision, servo-controlled balance was used for the hydrostatic weighing of solid objects. A mathematical derivation in Davis' paper permitted the precise calculation of the various volumes. The densities were then obtained by dividing the mass of each specimen by their corresponding calculated volumes.

V.3 Ultrasonic Measurements

Ultrasonic Velocity Test Specimens

The two large faces of each 4340 steel specimen were ground flat and parallel. one side of each specimen was then polished to a finish of 0.2 microns. The opposite side of the titanium alloy block, 5.08 cm x 5.08 cm x 1.91 cm, was polished to 0.2 microns. Each 0.2 micron finished 4340 steel specimen was then coupled with the 0.2 micron finished titanium block to provide several different interfaces to evaluate the sensitivity of Stoneley waves to microstructural changes as a function of interfacial bonding quality.

A second titanium block of similar dimensions was ground flat and parallel. This specimen was polished to a finish of 12 microns, and coupled with a 12 micron polished 4340 steel specimen in its as-received state. This pair was utilized to investigate the effects of surface finish on Stoneley wave velocity as a function of interfacial bonding quality.

Bulk Ultrasonic velocity measurements

There are several types of acoustic waves that propagate in a solid medium. Shear and longitudinal waves were two types of body waves used in this investigation. As a result of the two waves different propagation schemes, their measured velocities disclosed substantial information about the microstructure in various directions. The particle displacement of a longitudinal body wave is parallel to the direction of propagation, while that of a shear wave is perpendicular to the direction of propagation. By rotating a shear transducer 90°, the sampling direction of the particle displacement of a shear wave reveals the degree of anisotropy within a particular material. These measured velocities were then coupled with density values, and the elastic constants were calculated in the two different direction schemes. The four elastic parameters calculated in this investigation were Young's modulus (E), Shear modulus (G), Bulk modulus (B), and Poisson's ratio (υ) (Figure 9).

The technique employed to make time-of-flight measurements on shear and longitudinal waves was the pulse-echo overlap method. A Matec pulser-receiver was used as the wave generator and a Hewlett-Packard Amplitude-Scan Delta Time oscilloscope was used to measure the travel time between successive pairs of echoes. A light oil was used to couple a 5 MHz Panametrics longitudinal transducer with the steel and titanium ultrasonic samples for velocity measurements. A viscous silicone grease was used to couple a 5 MHz Panametrics shear transducer with the samples for shear velocity measurements. The maximum peak overlap convention was used throughout the bulk ultrasonic investigation because of its consistent time-of-flight readings.

Stoneley Wave Velocity Measurements

Theory suggested that Rayleigh waves generated in the denser medium would be mode converted to Stoneley waves at the point of intersection with an interface, if certain conditions were satisfied. The Stoneley wave would then propagate along the

$$\text{Young's Modulus (E)} = \rho \left[\frac{V_S^2 \left[3V_L^2 - 4V_S^2 \right]}{V_L^2 - V_S^2} \right]$$

$$\text{Shear Modulus (G)} = \rho V_S^2$$

$$\text{Bulk Modulus (B)} = \frac{E}{3\left[1 - 2\nu\right]}$$

$$\text{Poisson's Ratio } (\nu) = \frac{E}{2G} - 1 = \frac{V_L^2 - V_S^2}{2\left[V_L^2 - V_S^2\right]}$$

Figure 9. Equations used in calculations of elastic constant values. V_L is the longitudinal velocity, V_S is the shear velocity and ρ is the density.

interfacial boundary region until it encountered a free surface, whereupon it would reconvert into a Rayleigh wave.

In this investigation, several techniques were employed to generate and detect Stoneley waves. The first was a surface wave generation method. It involved the utilization of two broadband conical Industrial Quality, Inc.(IQI) transducers which launched surface waves over a very wide frequency range, D.C. to 2 MHz. Many problems were encountered with this technique. The two IQI transducers were used for both sending and receiving the surface waves. However, because of their broadband nature, they are usually only used for the receiving of acoustic signals. Another problem arose when trying to maintain point contact between the conical transducer and the sample. Several attempts included the use of c-clamps and a specially designed plastic mount. Both methods proved to be inefficient. Stoneley waves were also generated and detected by setting two longitudinal transducers at the corners of the base plate. The angles between the transducers and the base plate were varied to obtain the best wave forms. Clamps were used to hold the transducers at different angles. This method also proved to be inefficient because it was extremely difficult to find the angles that produced the highest resolution wave forms. Surface acoustic wave wedges were then employed to generate and detect Stoneley waves. Waveforms with high amplitude and relatively little noise were obtained. However, the exact travel distances were not easily measurable. Thus, the ultrasonic velocity values were inconsistent.

The technique utilized in this investigation for the generation and detection of Stoneley waves involved Rayleigh mode conversion wedges (Figure 10) [24]. Accurate wave path distances between successive echoes and waveforms of high resolution were easily obtainable by this method. The set-up included two-machined aluminum wedges in a sliding mount. Contact was made with the base plate through the knife-edge surfaces of the wedges. The critical angle between the wedge and the base plate measured to be approximately 60°. This critical angle provided the maximum mode-conversion efficiency for a longitudinal wave into a Rayleigh wave and the reverse conversion. Longitudinal piezoelectric transducers were mounted inside of each wedge for the sending and receiving of the acoustic waves. During ultrasonic testing, the titanium alloy block, dimensions 5.08 cm x 5.08 cm x 1.91 cm, was placed in the path of the generated Rayleigh wave. A hollow steel block was designed to allow the application of a compressive load perpendicular to the interface (Figure 11). The effect of interfacial bond quality on Stoneley wave velocity was then evaluated as a function of the applied stress. The tensile tester was capable of exerting 25 metric tons.

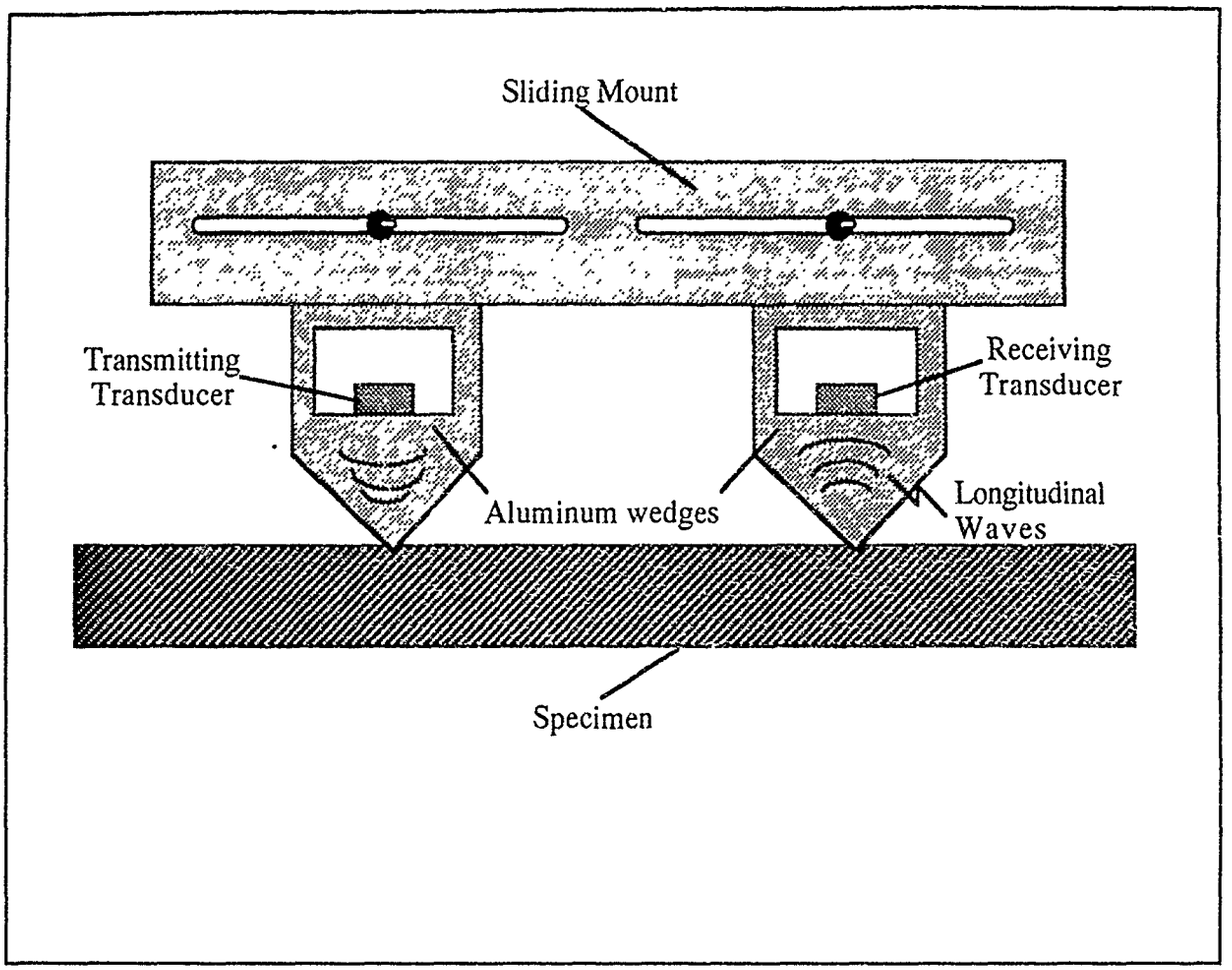

Figure 10. Schematic of wedges used to generate and detect Rayleigh surface

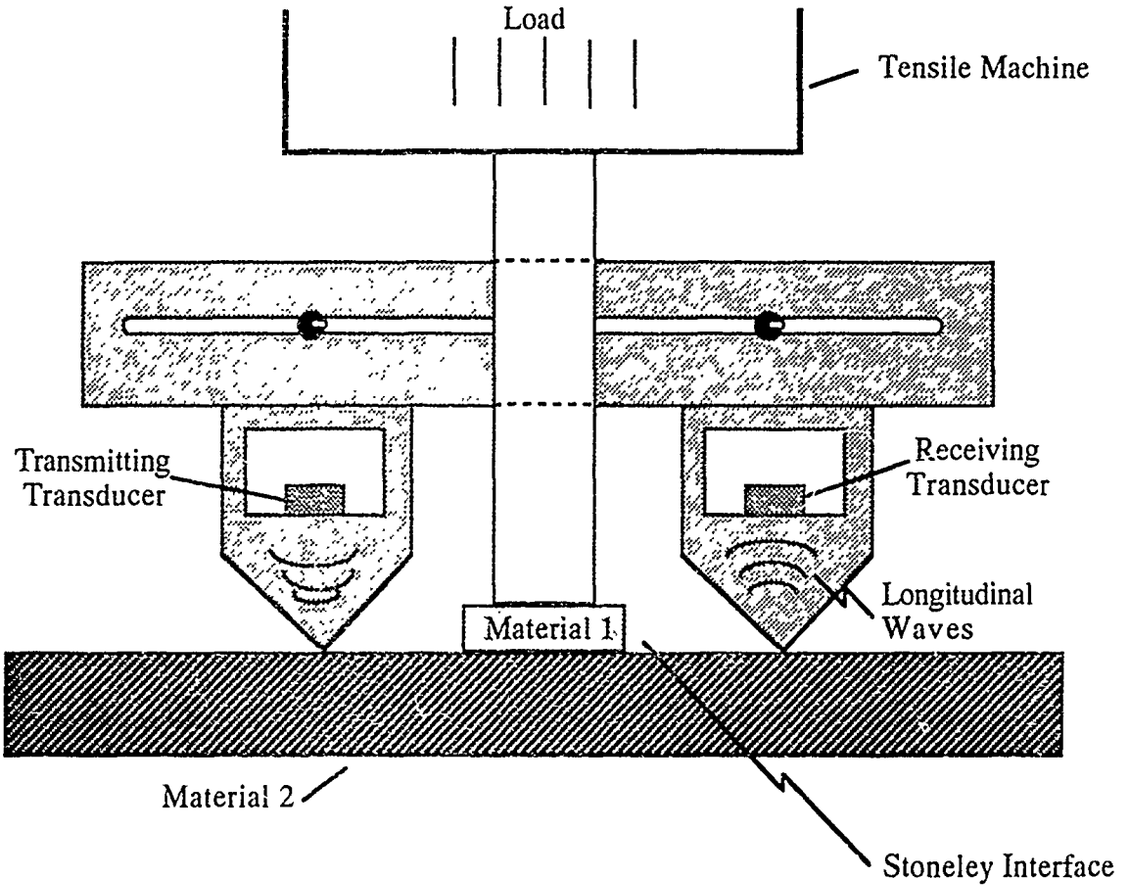

Figure 11. Schematic diagram of Stoneley wave set-up. Tensile test machine and modified steel block were used to investigate the effects of interfacial bond quality.

The standard ultrasonic set-up previously described was used to measure the time-of-flight of the Stoneley wave. The steps involved in the generation and detection of Stoneley waves are as follows. First, a longitudinal wave was piezoelectrically generated and propagated through one wedge. The longitudinal wave was then mode-converted to a Rayleigh wave at the point of contact with the base plate. This acoustic surface wave traveled along the base plate until it intersected the interfacial region, whereupon it mode-converted into a Stoneley wave. After the wave traveled across the boundary region, it reconverted into a Rayleigh wave at the intersection with the free surface and continued to the second wedge. At the point of contact with the wedge, the surface wave became a longitudinal wave and was subsequently detected by the second piezoelectric transducer. This technique is referred to as the pitch-catch method (Figure 12). The maximum peak overlap technique was used to make consistent time-of-flight measurements. Stoneley wave velocity readings were performed on all five 0.2 micron interfaces, and the corresponding Stoneley wave velocities were calculated using the equation in Figure 13. This procedure was also performed on the 12 micron finished interface to determine the effects of surface finish on Stoneley wave velocity. In both cases, these velocities were plotted as a function of the interfacial bond quality, as determined by the magnitude of the compressive load.

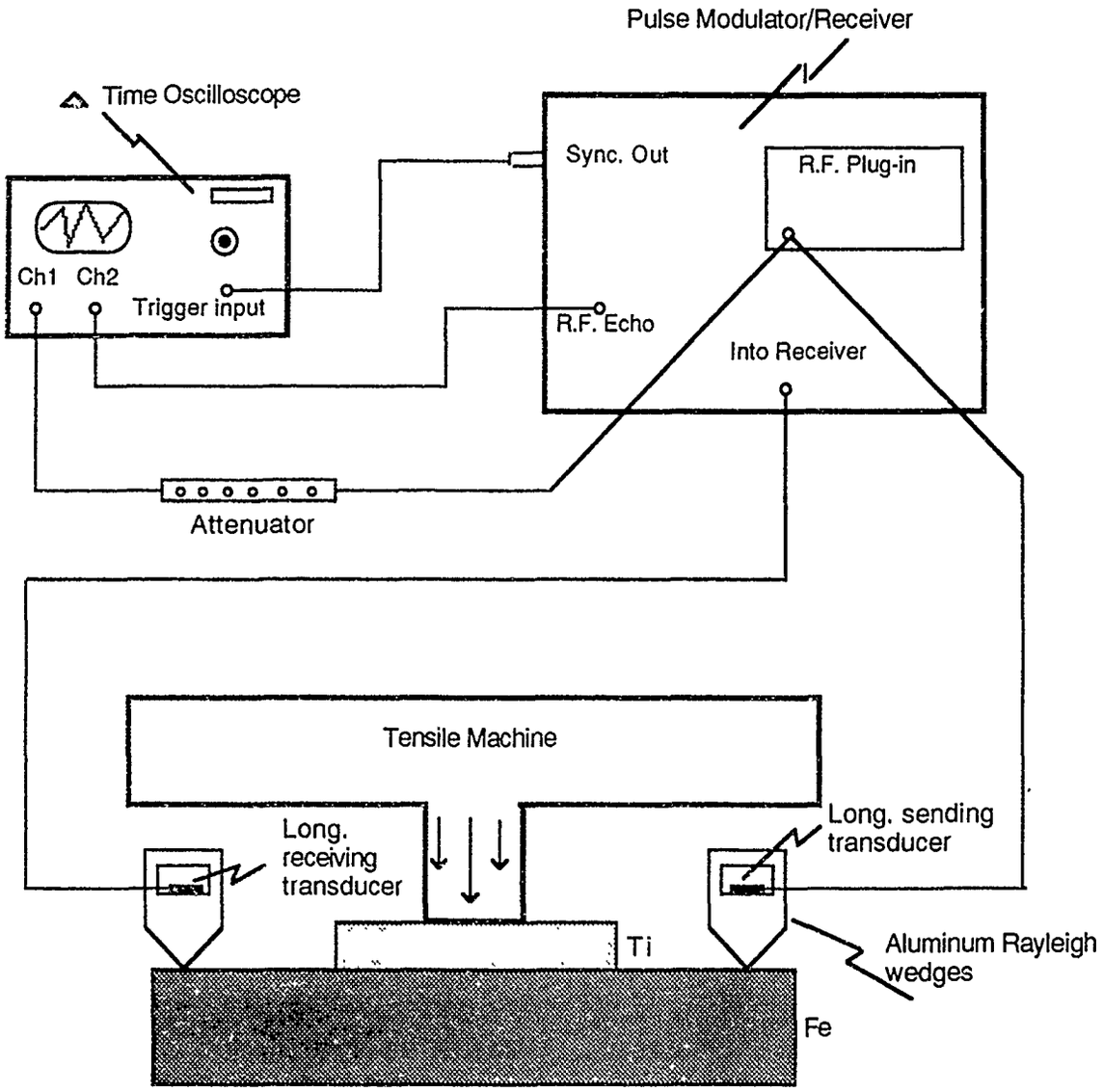

Figure 12. Experimental set-up used to measure the ultrasonic velocity of interface waves propagating on a steel/titanium interface.

$$\text{Velocity}_{ST} = \left[\text{Velocity}_{\text{Total}} - \text{Velocity}_{R} \frac{\text{Distance}_{R}}{\text{Distance}_{\text{Total}}} \right] \frac{\text{Distance}_{\text{Total}}}{\text{Distance}_{ST}}$$

Velocity $_{ST}$ = Stoneley velocity

Velocity $_{R}$ = Rayleigh velocity

Velocity $_{\text{Total}}$ = Total measured velocity, (Distance between wedges divided by calculated travel time)

Distance $_{R}$ = Distance travelled by Rayleigh wave on free surface

Distance $_{ST}$ = Distance travelled by Stoneley wave (length of interface region)

Distance $_{\text{Total}}$ = Total distance between wedges

* A travel time for the longitudinal waves in the wedges must be subtracted from the time reading on the digital display unit.

Figure 13. Equation utilized for the determination of Stoneley wave velocities.

V.4 Results and Discussion

The theory for Stoneley wave existence and the experimental background have been presented. The results of the sensitivity of Stoneley waves to microstructural variations will be examined. In addition, the effects of interfacial bonding quality and surface finish on Stoneley wave velocity will be determined and discussed.

Metallographic examination of the 4340 steel specimens revealed all five to have different microstructures (Figures 14-18). The photomicrograph in Figure 14 indicated the as-received specimen resembled a coarse pearlite within a ferritic matrix. The lamellar structure, pearlite, consists of alternating bands of alpha iron and iron carbide. The dark areas are iron carbide, and the ferritic matrix appears as the light colored regions. Similarly, specimen two, the austenitized and isothermally cooled sample, also contains partially spheroidized lamellar regions (pearlite) within a ferritic matrix (Figure 15). Comparison of the two microstructures revealed the pearlitic area of specimen one to be more defined. One possible cause for the larger extent of localized spheroidization within the pearlitic regions of specimen two, the coarser pearlite, may be the longer isothermal cooling periods it underwent. The photomicrograph of specimen three (Figure 16) indicated a fairly coarse martensitic structure, resulting from a rapid oil quench. Specimen four, the quenched and tempered steel, underwent nearly the same heat treatments as specimen three. In addition, a tempering process followed the quench. The photomicrograph (Figure 17) disclosed a microstructure that contained remnants of needle-like platelets of martensite that have been decomposed as a result of the tempering process. The photomicrograph of specimen five (figure 18) revealed a microstructure consisting of a conglomeration of coarse martensitic regions and small areas of bainite. Metallography of the titanium alloy was also performed to determine the grain texture. Its photomicrograph (Figure 19) showed the grains to be elongated in the rolling direction. The highly anisotropic microstructure suggested that ultrasonic behavior might vary in different directions. Consequently, in preliminary experiments, Stoneley waves were generated in directions parallel and perpendicular to the rolling direction.

Specimen one and two both have hardnesses indicative of a microstructure containing a mixture of pearlite and ferrite (Table I). Their two hardnesses are 96.2 R_B and 92.3 R_B respectively. One possible cause for the discrepancy in hardness values may be accounted for by the extent of spheroidization that has taken place within specimen two. Previous literature indicated that, for the same grade of steel,

spheroidization of the pearlitic regions causes a small decrease in hardness [25]. The hardenability profile of 4340 steel is pictured in Figure 20 [26]. It suggests a martensite quenched to approximately 98% will have a corresponding Rockwell C hardness of 56 to 58. Accordingly, specimen three, an almost fully quenched martensite, has an average hardness of 58.7 R_C. Specimen four has a lower average hardness value, 54.1 R_C This reduction in hardness verifies the tempering process specimen four underwent. Thus, the ductility of the steel was increased at the expense of the hardness. The lower hardness value 50.7 R_C for specimen five suggested the presence of small areas of bainite within a mostly martensitic matrix.

As expected, the density values for the pearlitic specimens are larger than those of the martensitic (Table I). Specimens one and two have density values of 7.839 grams/centimeter^3 and 7.840 grams/centimeter^3 respectively. Specimen three, the quenched martensite, has a density value of 7.807 grams/centimeter^3 , which is quite similar to specimen four's value of 7.805 3 grams/centimeter^3. The density value of specimen five,3 7.817 grams/centimeter^3 , is greater than the two other martensitic specimens but less than the two pearlitic. Close examination of the titanium alloy revealed its hardness and density values to be similar to those listed in previous literature [27]. The alloy had an average hardness of 33.1 R_C and a density of 4.430 grams/centimeter^3 .

The ultrasonic velocity measurements, in Table II, exhibited that longitudinal, shear, and Rayleigh waves travel with higher velocities within the pearlitic microstructures of 4340 steel than in those corresponding to martensites. In accordance with these results, previous literature suggested for the same grade of steel, that samples with higher hardness values generally correspond to lower ultrasonic velocities [28]. The consistency of the measured shear velocities in two perpendicular directions signified that the steel microstructures are not highly anisotropic. Further measurements on the titanium alloy disclosed a consistent longitudinal velocity, 6287.42 meters/second. The shear velocities measured parallel and orthogonal to the rolling direction vary to a large degree, and thus, the titanium alloy is highly anisotropic. The shear velocity measured in one direction is 3158.90 meters/second. The shear velocity, measured by rotating the transducer 90°, was found to equal 3276.22 meters/second.

The calculated elastic constants exhibited the same trends as the ultrasonic velocity values. The pearlitic microstructure yielded higher elastic constant values than the martensitic specimens (Table III-VII). Moreover, and as expected, the Poisson's ratio values of the martensitic specimens are larger than those of the two pearlitic specimens. The elastic constants of the titanium alloy in Table VIII vary significantly

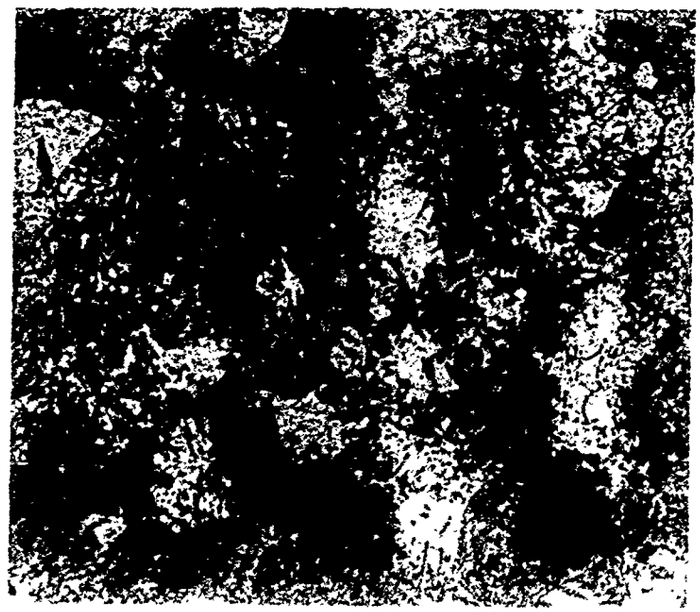

Figure 14. Specimen 1, the as-received sample. At 1000x. 2% Nital etch.

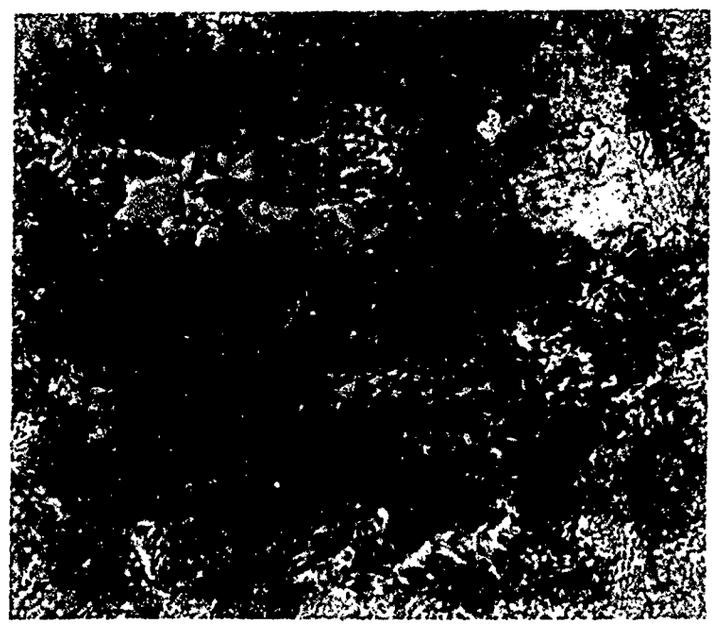

Figure 15. Specimen 2 after austenitizing at 843 C and isothermally cooling at 648 C for 48 hours. At 1000x. 2% Nital etch.

Figure 16. Specimen 3 after austenitizing at 843 C and quenching in oil.. At 1000x. 2% Nital etch.

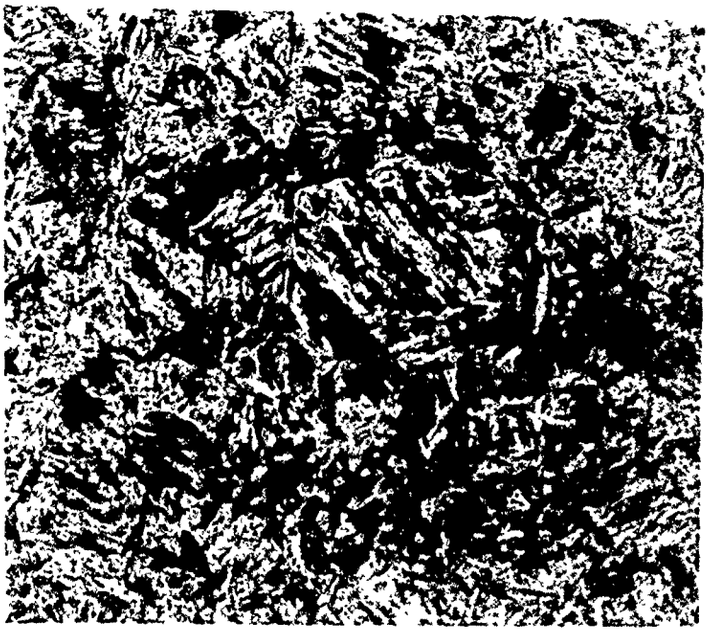

Figure 17. Specimen 4 after austenitizing at 843 C, quenching in oil and tempering at 204 C for 100 minutes. At 1000x. 2% Nital etch.

Figure 18. Specimen 5 after austenitizing at 843 C and air-cooling. At 1000x. 2% Nital etch.

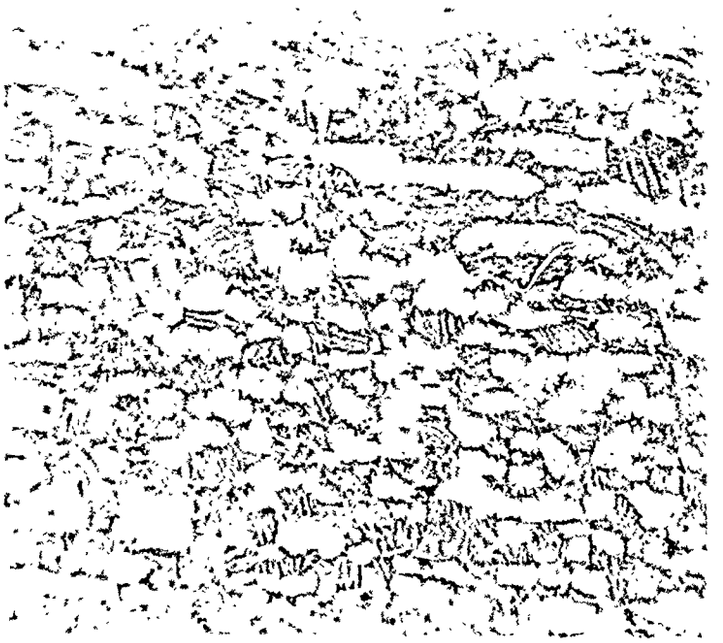

Figure 19. Titanium-6 Aluminum-4 Vanadium. Long axis of the grains coincide with the rolling direction. At 500x. Krolls Reagent etch.

Table 1- Hardness and Density Measurements

Specimen	Hardness	Density (g/cm^3)
1	96.2 R_B	7.839
2	92.3 R_B	7.840
3	58.7 R_C	7.807
4	54.1 R_C	7.805
5	50.7 R_C	7.817
Ti-6Al-4V	33.1 R_C	4.430

Table II- Ultrasonic Velocity Measurements

Specimen	Longitudinal Velocity (m/sec)	Shear Velocity 1 (m/sec)	Shear Velocity 2* (m/sec)	Rayleigh Velocity (m/sec)
1	5934	3235	3237	3000
2	5952	3250	3252	3005
3	5850	3156	3156	2909
4	5868	3170	3172	2931
5	5869	3175	3173	2935
Ti-6Al-4V	6287	3276	3159	-

*Measured by rotating transducer 90 .

Table III- Specimen 1 - Elastic Constants

	Calculated using shear velocity 1	Calculated using shear velocity 2	Average
Young's Modulus (E)	211,385	211,638	211,511
Shear Modulus (G)	82,020	82,147	82,083
Bulk Modulus (B)	166,666	166,492	166,579
Poisson's Ratio (ν)	0.289	0.288	0.288

Table IV- Specimen 2 - Elastic Constants

	Calculated using shear velocity 1 MPa	Calculated using shear velocity 2 MPa	Average MPa
Young's Modulus (E)	213,307	213,418	213,362
Shear Modulus (G)	82,839	82,895	82,867
Bulk Modulus (B)	167,281	167,209	167,245
Poisson's Ratio (ν)	0.287	0.287	0.287

Table V- Specimen 3 - Elastic Constants

	Calculated using shear velocity 1 MPa	Calculated using shear velocity 2 MPa	Average MPa
Young's Modulus (E)	201,373	201,384	201,378
Shear Modulus (G)	77,768	77,775	77,771
Bulk Modulus (B)	163,481	163,727	163,604
Poisson's Ratio (ν)	0.295	0.295	0.295

Table VI- Specimen 4 - Elastic Constants

	Calculated using shear velocity 1 MPa	Calculated using shear velocity 2 MPa	Average MPa
Young's Modulus (E)	202,994	203,158	203,076
Shear Modulus (G)	78,445	78,527	78,486
Bulk Modulus (B)	164,126	164,012	164,069
Poisson's Ratio (ν)	0.294	0.294	0.294

Table VII- Specimen 5 - Elastic Constants

	Calculated using shear velocity 1 MPa	Calculated using shear velocity 2 MPa	Average MPa
Young's Modulus (E)	203,791	203,557	203,674
Shear Modulus (G)	78,801	78,683	78,742
Bulk Modulus (B)	164,167	164,306	164,236
Poisson's Ratio (ν)	0.293	0.293	0.293

Table VIII- Titanium-Aluminum-6-Vanadium-4 - Elastic Constants

	Calculated using shear velocity 1 MPa	Calculated using shear velocity 2 MPa	Average MPa
Young's Modulus (E)	124,925	117,688	121,306
Shear Modulus (G)	47,550	44,205	45,877
Bulk Modulus (B)	111.710	116,174	113,942
Poisson's Ratio (ν)	0.314	0.331	0.322

with direction measured and are characteristically lower than the 4340 steel values. The Poisson's ratios are larger than those of the 4340 steel, but the anisotropy within the specimen causes a large deviation between the parallel and orthogonal directions, 0.331 and 0.314.

The experimentally calculated results of Weichert's condition for the various 4340 steel samples and the titanium alloy couple appear in Table IX. The values for the ratios of the densities and ratios of the shear modulus are calculated to determine the possible range of existence for Stoneley waves along the interface according to Sezawa and Kanai's graphical depiction in Figure 2. The ratios of the densities vary between 0.565 and 0.567, while the ratios for the shear modulus ranges from 0.52 to 0.60. Theoretically, if the point plotted according to the two ratios, for each interfacial couple, is within the two curves (Figure 2), then Stoneley waves will exist along the interface. This approximation of Weichert's condition is satisfied for the two pearlitic-titanium couples. Both ratios for the densities of the two media were calculated and equal 0.565. The ratios for the shear modulus in the two media comprising the interface were found to differ in two perpendicular measured directions. This arose as a result of the anisotropy present within the titanium alloy block. However, both measured shear modulus orientations provided ratios that satisfied the range of existence for Stoneley waves according to the approximation made by Sezawa and Kanai. The ratios of the densities for the interfaces comprised of specimen three, four, and five were calculated and equal 0.567 for three and four and 0.566 for specimen five. once again, the ratio of the shear modulus in two perpendicular directions was calculated for the samples. The ratios of the shear modulus measured perpendicular to the rolling direction of the titanium block exhibited values of 0.611, 0.606, and 0.604 for specimens three, four, and five, respectively. When taken in conjunction with the calculated density ratios, all three plotted points seem to be near the upper limit for the possible range of existence for Stoneley waves. However, the ratios of the shear modulus measured parallel to the rolling direction of the titanium block revealed values that are approximately equal to the three density ratios. These three measured shear modulus ratios are 0.568 for the interface comprised of specimen three, 0.563 for the interface comprised of specimen four, and 0.561 for that of specimen five. When combined with the density ratios for their respective material combinations, all three plotted points are well within the possible range of existence for Stoneley waves along the interfacial region. It is believed this approximation of Weichert's condition held true during experimentation. During ultrasonic testing, a shear wave transducer was placed on the side of the lighter medium (in this experimentation, the titanium block) to detect the possible existence of leaky

Specimen #	Density medium 1 / Density medium 2	Shear Modulus med 1* / Shear Modulus med 2	Shear Modulus med 1** / Shear Modulus med 2
Density = 7.839 g/cm^3 Ave. Shear Modulus = 82,083 MPa	0.565	0.579	0.538
Density = 7.840 g/cm^3 Ave. Shear Modulus = 82,867 MPa	0.565	0.574	0.533
Density = 7.807 g/cm^3 Ave. Shear Modulus = 77,771 MPa	0.567	0.611	0.568
Density = 7.805 g/cm^3 Ave. Shear Modulus = 78,486 MPa	0.567	0.606	0.563
Density = 7.817 g/cm^3 Ave. Shear Modulus = 78,742	0.566	0.604	0.561

*Calculated using Shear Velocity 1 in Titanium Alloy
**Calculated using Shear Velocity 2 in Titanium Alloy

Table IX - Experimental ratios between the densities and shear modulus of the two media comprising the interfacial region. Titanium (density = 4.43 g/cm)
Titanium shear modulus: direction 1 = 47,550 MPa, direction 2 (transducer rotated 90°) = 44,205 MPa

waves along the interface. If leaky waves were present, the shear wave transducer would receive a signal, thus indicating the presence of shear wave displacement fields within the lighter material. For all five experimental material combinations, there was no indication of this phenomenon.

The depiction by Yamaguchi and Sato of the relationship between densities, shear modulus and interface wave velocities enabled the determination of theoretical Stoneley velocities [10]. For each material combination in this investigation, the ratio of the densities and the ratio of the shear modulus were plotted on the horizontal and vertical axes, respectively. A theoretical value for the ratio of the maximum Stoneley wave velocity to the shear wave velocity, quantity squared, could then be obtained upon extrapolation. This ratio was determined to equal approximately 0.995 for all five interfacial combinations. Subsequently, each theoretical Stoneley velocity was obtained by multiplying each steel's average shear velocity by 0.997 (Table X). As expected, the two interfaces comprised of the pearlitic specimens exhibited higher theoretical Stoneley wave velocities than the three containing the martensitic samples.

The ability of Stoneley waves to detect variations in microstructure was evaluated on the five 0.2 micron finished titanium-steel couples. For each experimental interface, the Stoneley wave velocities were calculated as a function of interfacial bond quality. Through the utilization of a tensile test machine, a compressive load was applied perpendicular to each interface. It was hypothesized that as the pressure was increased, the interface would change from a boundary region with finite areas of contact to one of continuous contact. Thus, with each increment of air gap elimination, the interface wave would travel with higher velocities. Eventually, when continuous contact between the two adjoining surfaces was achieved, a maximum would be reached corresponding to the Stoneley wave velocity. Subsequently, a correlation could be made between the Stoneley wave velocity and the quality of the interfacial region as determined by the magnitude of the applied pressure. Experimentally, this was accomplished by plotting the Stoneley wave velocity versus the normalized stress for each steel-titanium couple. The normalized stresses were taken to equal the applied stress, force per unit interfacial area, divided by the yield stress of each steel specimen. The approximate yield stresses were obtained by utilizing several tables that converted Rockwell hardnesses for a specific heat treatment to yield strengths [29]. The yield stresses are as follows:

Table X- Theoretical and Experimentally Measured Stoneley Wave Velocities

Interface comprised of Titanium and Specimen #	Theoretical Stoneley Velocity (m/sec)	Experimentally Measured Stoneley Velocity (m/sec)
1	3226	3210
2	3241	3220
3	3146	3085
4	3161	3155
5	3173	3160

Specimen one	=	70 ksi
Specimen two	=	55 ksi
Specimen three	=	225 ksi
Specimen four	=	225 ksi
Specimen five	=	150 ksi

Because of the anisotropy present within the titanium alloy block, Stoneley wave velocities were measured in two directions, one coinciding with the blocks rolling direction and the other by rotating the block 90°. The most consistent results were obtained when the Stoneley waves traveled through the interface parallel to the rolling direction of the titanium block.

The characteristic Stoneley wave velocities of the two pearlitic specimens versus normalized stress profiles are depicted in Figure 21. At zero applied pressure, corresponding to the vertical axis, the Stoneley wave velocity of specimen one nearly equaled the Rayleigh wave, 2995 meters/second. As the pressure was increased, the interfacial bond quality was improved, and the Stoneley wave velocity increased asymptotically to a maximum of 3210 meters/second. Comparison of this experimentally measured value with Yamaguchi and Sato's approximated theoretical Stoneley velocity of 3226 meters/second, suggested the interfacial region may be approaching full continuity at the maximum applied pressure. The Stoneley wave velocity of specimen two also increased asymptotically with improved interfacial bonding, from its measured Rayleigh velocity of 3005 meters/second to approximately 3220 meters/second. However, a small discrepancy at the lower end of the curve is believed to exist as a result of the surface finish on the steel. Although specimen two was provided with a 0.2 micron finish, the surface was accidentally allowed to corrode slightly. Consequently, small surface inconsistencies were present and these effects tended to move the immediate rise in interface wave velocity with increasing pressure to the right. Initially, higher applied pressures were necessary to bring the two adjoining media into intimate contact because of the rough surface finish on specimen two. At the upper end of the curve, it appears the Stoneley velocity has not reached its maximum value. Extrapolation of this curve would produce a Stoneley wave velocity of slightly higher magnitude and closer in value to the approximated theoretical prediction of 3241 meters/second. Experimentally it is believed the measurable Stoneley wave velocity would increase with the application of higher pressures and the subsequent

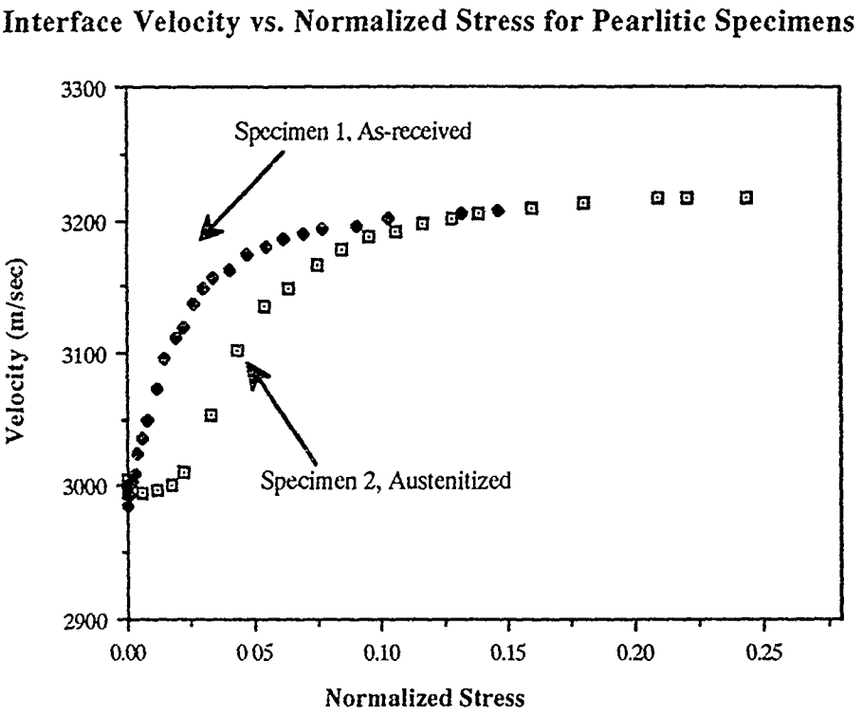

Figure 21. Stoneley velocity versus normalized stress for pearlitic specimens. Stress normalized to yield stress, Specimen 1- 70 ksi, Specimen 2- 55 ksi.

improvement of the interfacial bond quality. In retrospect, all of measured elastic acoustic waves propagate in specimen two with higher velocities than in specimen one. Both curves in Figure 21 seemed to reach their maximum Stoneley velocities at approximately 0.25 of their normalized stresses. A more complete analysis of the stresses required to form an interfacial region suitable for the propagation of Stoneley waves could not be determined because of the accidental surface variation on specimen two.

The Stoneley wave velocities of the martensitic specimens versus normalized stress profiles are depicted in Figure 22. All three experimentally measured Stoneley wave velocities are lower than the two pearlitic values. Individually, the Stoneley wave velocity for each martensitic-titanium couple increased with improving interfacial bond quality in a different manner. At zero applied pressure, the Stoneley wave velocity of specimen three (quenched martensite) was 2910 meter/second, corresponding to a Rayleigh surface wave traveling on the steel plate. As the pressure was increased, the interfacial bond quality improved, thus causing the elastic wave to be transmitted through the boundary region with higher velocities. Eventually, the Stoneley wave reached an experimental maximum velocity at 3085 meters/second. However, the slope of the curve appeared to be still rising at approximately 0.06 normalized stress. It was speculated that the Stoneley velocity did not approach a maximum in this case because the tensile tester used in this investigation was not capable of exerting the higher stresses necessary to bring the martensitic steel and titanium alloy into complete contact. If complete contact of this continuous interfacial region occurred, it is believed a Stoneley wave would propagate through the interface with higher velocities. Theoretical predictions indicated the Stoneley wave would propagate at 3146 meters/second. Since the tempered steel, specimen four (R_C = 54.1), is softer than the quenched steel (R_C = 58.7), lower applied stresses were needed to form the necessary continuous interface for the propagation of Stoneley waves. As with the other steel specimens, the interface comprised of specimen four and the titanium alloy also had an interface wave propagating along the boundary region with a velocity equal to its Rayleigh wave at zero applied pressure, 2930 meters/second. Within this interface couple, the Stoneley wave reaches higher velocities at lower normalized stresses. After the initial rise in velocity the curve leveled off asymptotically at approximately 3155 meters/second. Theoretically, a velocity of 3161 meters/second was calculated. Comparison of these two values indicated the controlled interface may not have achieved full continuity. However, the same patterns in velocity measurements were observed as in previous experiments. Namely, longitudinal, shear, Rayleigh, and Stoneley waves were all measured to travel

Interface Velocity vs. Normalized Stress for Martensitic Specimens

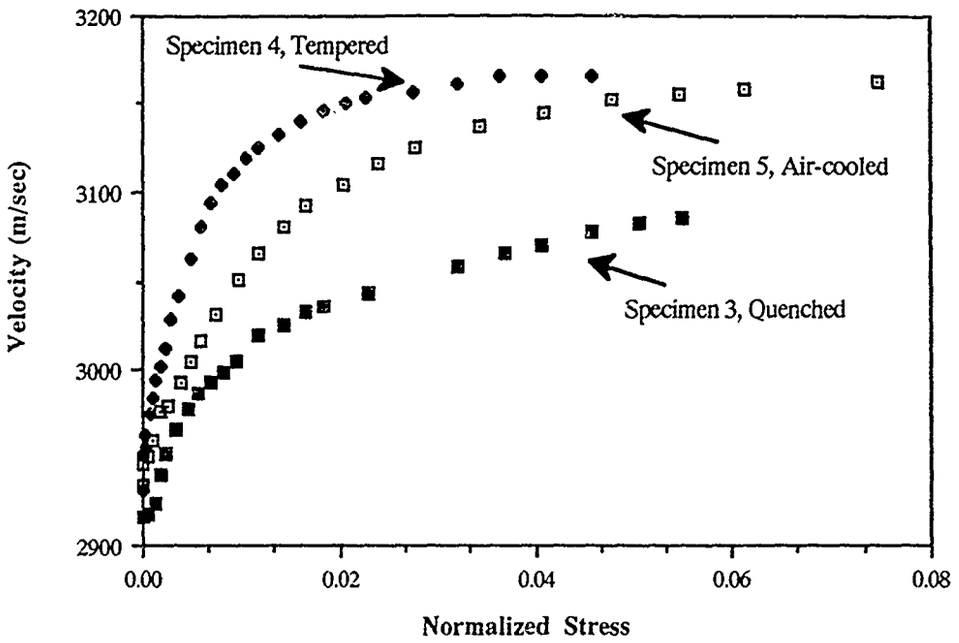

Figure 22. Stoneley velocity versus normalized stress for martensitic specimens. Stress normalized to yield stress, Specimen 3- 225 ksi, Specimen 4- 225 ksi, Specimen 5- 150 ksi.

with higher velocities in specimen four than in specimen three. The interface comprised of specimen five, the air-cooled sample, and the titanium alloy had a Stoneley velocity versus normalized stress profile similar to specimen four. In agreement, the shear, longitudinal, and Rayleigh waves all propagated with nearly equal velocities in each of these material combinations. The dissimilarities between the initial rise in velocity with applied stress in specimens four and five is unclear. It is believed that higher applied stresses might allow for a clearer distinction between the two specimens. In comparison with specimen three, lower applied stresses were needed to form the necessary continuous interface. This was attributed to the lower hardness of specimen five (R_C = 50.7). At the upper end of the curve the Stoneley wave velocity experimentally reached a value of 3160 meters/second. The theoretically determined Stoneley velocity of 3173 meters/second is also slightly higher in value than the theoretically calculated value for the tempered martensite-titanium couple. Once again, the lower experimental velocity suggested the interface may not be fully continuous as a result of the hardness of martensitic steel. Thus, it was hypothesized for the martensitic steel couples that an acoustic wave was not capable of being transmitted along the boundary region with a velocity indicative of a Stoneley wave. Higher applied pressures may possibly cause the interfacial region to improve and subsequently increase the maximum velocities attained by the interface wave. All three Stoneley waves traveling through the martensitic couples were observed to reach their experimental maximums between 0.05 and 0.08 their normalized stresses. These reduced values in normalized stress, in comparison to the pearlitic couples, arose because of the martensitic specimens higher yield strengths.

In further investigations, Stoneley waves were generated between a 12 micron finished as-received 4340 steel sample and titanium alloy of the same finish. The Stoneley wave velocity versus the normalized stress profile is depicted in Figure 23. Once again, at zero applied pressure to the interface, an acoustic wave was measured to propagate between the 12 micron finished couple with a velocity nearly equal to a Rayleigh wave on the steel sample. However, as the pressure was increased there was not an immediate rise in interface wave velocity. This behavior suggested that higher applied pressures are needed to bring the two comparatively rougher surfaces into intimate contact. Accordingly, it was speculated that poor surface finish may cause an acoustic wave to travel along the interface with velocities only slightly higher than a Rayleigh wave. Increases in interface wave velocity were not observed until approximately 0.15 of the normalized stress. In comparison, the 0.2 micron finished couple demonstrated an immediate rise in Stoneley wave velocity with applied

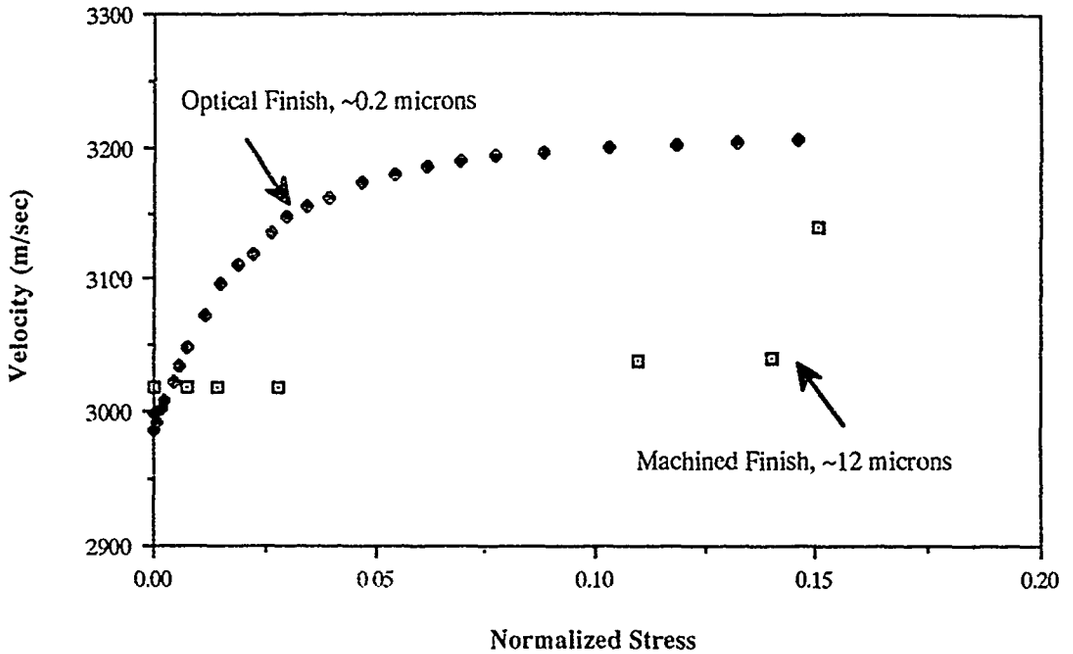

Figure 23. Effect of surface finish on Stoneley wave velocity.

pressure. The two profiles suggest interfaces comprised of optically finished surfaces require less force to attain a continuous boundary region necessary for the propagation of Stoneley waves than do interfaces comprised of comparatively rougher adjoining surfaces.

In this investigation, the sensitivity of Stoneley waves to interfacial bond quality was examined as a function of applied stress, surface finish and variations in microstructure. For all six experimental couples, the interface wave was observed to propagate with a velocity indicative of a Rayleigh wave at zero applied pressure. In the five 0.2 micron finished couples, the successive elimination of air gaps and the subsequent improvement of the interfacial bond quality caused the interface wave velocity to increase asymptotically to a maximum value nearly equal to the theoretical Stoneley velocity. The effects of surface finish revealed an acoustic wave traveled along the boundary region with velocities only slightly higher than a Rayleigh wave for poorly finished (12 micron) surfaces at low and intermediate pressures. Upon comparison with the 0.2 micron finished surfaces, higher applied stresses were required to cause a small increase in the interface wave velocity for the rougher surfaces. Thus, the effects of surface finish suggest that an interface comprised of finely polished surfaces required lower stress to form the necessary continuous boundary region for the propagation of Stoneley waves than do rougher surfaces.

In summation, it is believed that Stoneley waves may be used to evaluate the coherency and integrity of an interfacial region. Moreover, the various calculated Stoneley velocities indicated that interface wave velocity measurements are sensitive to microstructural variation and surface finish. Namely, Stoneley waves traveled through the two pearlitic steel-titanium interfaces with higher velocities than in the three martensitic steel-titanium couples. The effects of surface finish indicated that surfaces with better finishes require less force to attain the necessary continuous boundary region for the propagation of Stoneley waves.

V.5 Conclusions

- Stoneley interface waves were generated and detected between steel-titanium planar interfaces.

- Stoneley interface waves were found to be sensitive to changes in microstructure. Interface waves propagated through the pearlitic 4340 steel-titanium interfaces with greater experimental Stoneley interface wave velocities than through the martensitic 4340 steel-titanium interfaces. Interface waves propagated with higher velocities through steel-titanium interfaces of good surface finish than they did through steel-titanium interfaces comprised of poorly finished surfaces. Interface wave velocities were found to be dependent on the quality of the interfacial bond. It was hypothesized that as the pressure applied to the interface was increased, the interface would change from a boundary region with finite areas of contact to one of continuous contact. Thus, with each increment of air gap elimination, the interface wave would travel with higher velocities. Upon achievement of continuous contact between the two adjoining surfaces, a maximum velocity would be reached corresponding to that of a Stoneley wave. The interface waves were observed to propagate through the steel-titanium interfacial regions with a velocity corresponding to a Rayleigh wave at zero applied pressure. As the pressure applied to the interface was increased, the interface wave velocities increased asymptotically to a maximum that was slightly less than theoretical predictions. Through the utilization of Yamaguchi and Sato's method for predicting Stoneley interface wave velocities, interface waves were theoretically calculated to propagate through the two pearlitic steel-titanium interfaces with higher velocities than through the three martensitic steel-titanium interfaces.

- The five steel-titanium interfacial couples were tested to evaluate the possible existence of leaky waves along the boundary region. For all five material combinations, there was no observable detection of this phenomena.

VI. Leaky wave Prpoagation for NDE

VI.1 Introduction

The previous experiments demonstrate the feasibility of generating both Stoneley and leaky waves at a planar solid-solid interface through mode conversion. In addition, theoretical analysis allowed particle motion, energy flow, and velocity predictions for comparison to experimental results. It was shown that interface waves were sensitive to microstructural variation as well as quality of surface contact. These microstructural effects which caused small changes in elastic properties are manifested as changes in ultimate interface wave velocity and were measured simply and accurately.

The problems of expanding this research to include more relevant engineering material pairs are numerous. It is obvious from the theoretical analysis that the limited region of existence of Stoneley waves makes it impractical for nondestructive characterization of many composite materials. Leaky waves which exist for a much larger range of material pairs, including silicon carbide/aluminum, seem to offer much more potential as a nondestructive evaluation tool. However, the lack of previous work and the limited theoretical analysis of these waves forced a fundamental approach to the problem. The approach taken in this study consisted of several experimental projects designed with specific, but related goals. The first is an experiment to further our understanding of basic leaky wave propagation characteristics. While some theoretical analysis exists, experimental observation and understanding is limited. The goal was not only to generate and detect leaky waves, but to measure the leakage and determine its potential for interface characterization. The second part of this project was to develop a technique to remotely generate and detect leaky waves in order to address the problem of interface access when mode conversion at free surface is not feasible. Once these problems are overcome, techniques for nondestructive evaluation of interface elastic properties may be developed utilizing leaky interface waves.

VI.2 Theoretical Considerations

In order to understand the experimental approach taken to examine the potential usefulness of leaky waves for nondestructive evaluation of interfaces, Stoneley's equation for phase velocity along an interface must be scrutinized. The original equation given in 1924 is,

$$c^4\left\{(\rho_1-\rho_2)^2-(\rho_1A_2+\rho_2A_1)(\rho_1B_2+\rho_2B_1)\right\}$$
$$+2Kc^2\left\{\rho_1A_2B_2-\rho_2A_1B_1-\rho_1+\rho_2\right\}$$
$$+K^2(A_1B_1-1)(A_2B_2-1)=0 \qquad \text{eq(1)}$$

where,

$$A_1=\left(1-c^2/V_{S1}^2\right)^{1/2} \qquad A_2=\left(1-c^2/V_{L2}^2\right)^{1/2}$$
$$B_1=\left(1-c^2/V_{S1}^2\right)^{1/2} \qquad B_2=\left(1-c^2/V_{S2}^2\right)^{1/2}$$
$$K=2\left(\rho_1V_{S1}^2-\rho_2V_{S2}^2\right) \qquad \text{eq(2)}$$

V_L and V_S are the longitudinal and shear wave velocities, ρ is the density, and the subscripts 1 and 2 refer to the two media. Medium 2 is defined as the more dense medium.

To further investigate this equation the concept of a Riemann surface must be introduced. A Riemann surface is a geometrical device which allows the complexities of a multiple-valued function to be more easily handled [30]. It is defined as a generalization of the z plane to a surface of more than one sheet such that the multiple valued function has only one value corresponding to each point on that surface. The surface is composed of sheets which correspond to a branch of the function, so that on each sheet the function is single-valued. The advantage of the Riemann surface is that the various values of multiple-valued functions are obtained in a continuous fashion.

From equation 1, it can be seen that there are 16 possible combinations of signs of the functions A_1, A_2, B_1, and B_2. Since changing all of the signs would leave the equation unaltered, there are only 8 which are independent. Each of these eight independent Riemann sheets was investigated by Pilant [11] for the presence of real or complex roots out to a radius where $|c^2| / V_{S2}^2 = 64$. Following his notation, a sign convention is chosen so that the real part of B_2 is always positive. The sign convention for the eight Riemann sheets then, is given as $Re\{A_1\}$, $Re\{B_1\}$, $Re\{A_2\}$. Using this notation, (+ - +) means that $Re\{A_1\}>0$, $Re\{B_1\}<0$, $Re\{A_2\}>0$ and $Re\{B_2\}$ is always >0. For a continuous cyclic variation in material parameters it was determined that there were 16 roots which could be followed about the various Riemann surfaces.

Before considering the case of an aluminum/silicon carbide interface, the general behavior of the sixteen roots as presented by Pilant was reviewed. Each of the roots was followed as the ratios of the shear velocities and the densities were varied in a half-

square as shown in Figure 24. Poisson's ratio is defined as 0.25 for both materials with material 2 designated as the denser of the two. Beginning with $(V_{S2}/V_{S1})^2$ and ρ_1/ρ_2 = 1, the density ratio was decreased to 0.5. The velocity ratio was then increased to 2.0 and finally the density ratio was increased back to 1.0. The graphical representation of the results are shown in Figure 25. Three points on this figure are of specific interest. At the first point , $(V_{S2}/V_{S1})^2 = 0.5$ and $\rho_1/\rho_2 = \sqrt{2}/2$ both real and complex roots become very large or go through the point at infinity and return with opposite sign. The second point, $(V_{S2}/V_{S1})^2 = 0.5$ and $\rho_1/\rho_2 = .05$ shows that many of the root values are zero on different Riemann sheets. The third combination is the pair $(V_{S2}/V_{S1})^2 = 1$ and $\rho_1/\rho_2 = .05$. At this point many of the roots have a value of 4 including a double root on the (+ - -) sheet. In this range of parameters, the only real root was the Stoneley root on the (+ + +) sheet. It is also clear that although the roots jump from sheet to sheet as the parameters are varied, the number of roots remains constant. Notice that in Figure 25 vertical tangents appear on the solid lines representing two real roots converging on the real axis which become a complex conjugate pair. Conversely, two complex conjugate roots meeting on the real axis create two real roots.

The boundary condition matrix equation for the planar interface case was examined in detail by Lee and Corbly [16] and Simmons and Krasicka [31]. Simmons and Krasicka extended the work of Lee and Corbly on cylindrical interfaces. To examine a planar interface, the radius of curvature was set to infintiy. If the z axis of a rectangular Cartesian system is defined to lie in the plane interface between two materials and the x axis is defined to extend into the less dense material, the displacement fields u_m are given by,

$$u_m=\nabla\varphi_m+\nabla x\left(0,\psi_m,0\right)$$

where eq(3)

$$\begin{aligned}\phi_1&=\alpha\exp\left(-kA_1x+ikz-i\omega t\right)\\ \psi_1&=\beta\exp\left(-kB_1x+ikz-i\omega t\right)\\ \phi_2&=\gamma\exp\left(kA_2x+ikz-i\omega t\right)\\ \phi_2&=\gamma\exp\left(kA_2x+ikz-i\omega t\right)\end{aligned}$$

eq(4)

where

$$A_m=\left(1-c^2/a_m^2\right)^{1/2}$$

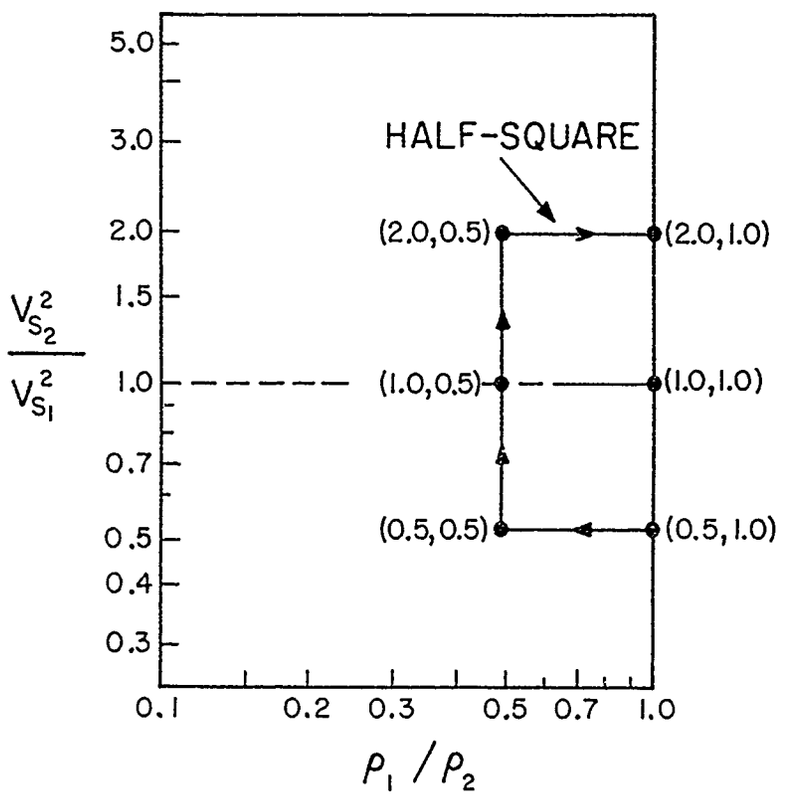

Figure 24. The path of variation of the parameters chosen by Pilant to evaluate the 16 roots of the equation governing elastic wave propagation on a solid-solid interface. Poisson's ratio is kept at 0.25, r is the density, and V_S is the shear wave velocity. Medium 2 is defined as the denser material.

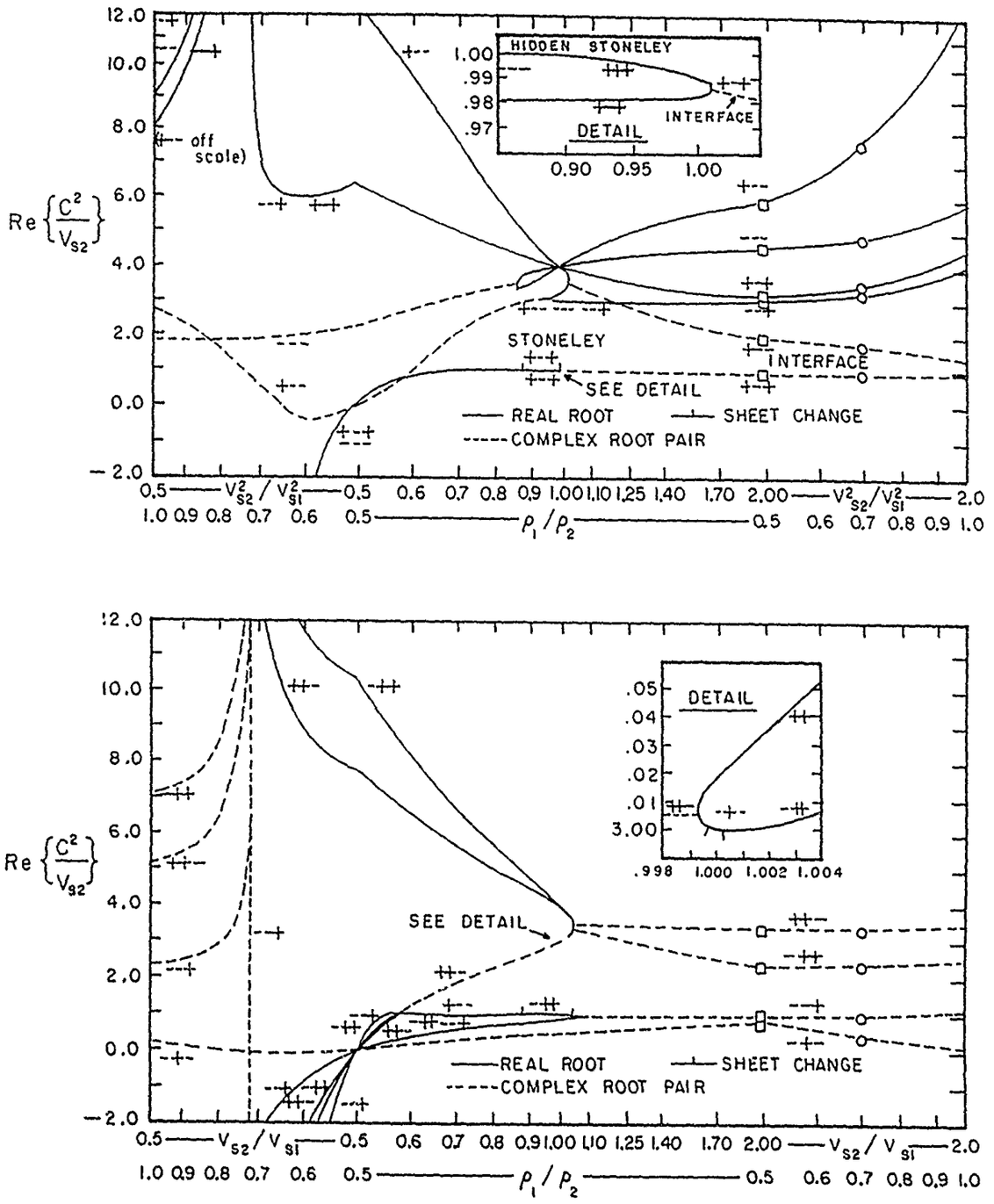

Figure 25. Graphical representation of the behavior of the 16 roots of the Stoneley equation as a result of varying the parameters over the half-square shown in Figure 24.

$$B_m=\left(1-c^2/b_m^2\right)^{1/2}$$
$$c=\omega/k \qquad \text{eq(5)}$$

The subscript m represents the two materials where 1 denotes the less dense and 2 denotes the denser material. The longitudinal and shear wave velocities are a_m and b_m respectively. When the boundary conditions of continuity of normal tractions and displacements at the interface is imposed the characteristic matrix takes the form shown below in Equation 6.

In order to study the Al/SiC system, experimentally determined values were substituted into the determinant and the following analytical results were obtained utilizing computer models at the National Institute for Standards and Technology. A double index notation was used, referring to s, t modes where s, t = 2p + q. Both p and q may be 0 if the negative principal square root value is chosen or 1 if the positive principal square root value for the longitudinal (p) and shear (q) components. Therefore, s and t range from 0 to 3. The first index refers to the matrix material, aluminum in this case and the second index to the reinforcing material, silicon carbide.

$$\begin{pmatrix} 2\rho_1 b_1^2 A_1 & 2\rho_2 b_2^2 A_2 & \rho_1 b_1^2\left(2-c^2/b_2^2\right) & \rho_2\left(2-c^2/b_2^2\right) \\ \rho_1\left(c^2-2b_1^2\right) & -\rho_2\left(c^2-2b_2^2\right) & -2\rho_1 b_1^2 B_1 & 2\rho_2 b_2^2 B_2 \\ 1 & -1 & B_1 & -B_2 \\ A_1 & A_2 & 1 & 1 \end{pmatrix} \begin{pmatrix} \alpha \\ \gamma \\ i\beta \\ -i\delta \end{pmatrix} = 0$$

eq (6)

All 16 branches of the matrix equation can produce solutions, however, not all solutions may physically exist. Leaky waves were calculated by NIST from Equation 3 by locating the approximate real and pure imaginary roots and then using Newton's method for computing the real and complex roots. Solution to the boundary matrix produces two types of modes. Decomposable modes which are a superposition of a longitudinal and shear plane waves and non-decomposable modes. The decomposable modes represent certain reflection/refraction situations in which one or more output wave is missing. Table XI shows the 10 interface modes for the SiC/Al system as calculated at NIST. There are six non-decomposable modes and four decomposable modes that appear.

Table XI

Nondecomposible Leaky Waves in Al/Sic		
Type	Velocity: Real part, imaginary part	Asymtotic Leakage Angle in Al
0,3	5562,1113	21.0
1,3	8643, 2458	49.0
2,3	4730, 231	49.2
1,1	4619, 3416	48.3
3,1	10481, 2454	-73.8
3,0	5562, 1113	-57.9

Decomposible Leaky Waves in Al/SiC					
Type	Velocity	Longitudinal Wave Angle		Shear Wave Angle	
		in Al	in SiC	in Al	in SiC
0,3	10030	50.9	15.8	72.0	58.8
2,3	10077	-51.3	16.8	72.0	59.0
3,2	11531	-56.7	33.2	-74.4	-63.2
2,1	16377	-67.3	-53.0	79.0	71.5

In order to better visualize these analytically determined leaky waves, Figures 26 and 27 show the energy flow and particle displacement for a non-decomposable and a decomposable type wave. The ellipses represent the shape of the particle orbit at a number of points with the arrowheads indicating the sense of the particle motion. The arrow from the center of the ellipse shows the energy flow or Poynting vector averaged over one period. Although the ellipse sizes and arrow lengths are arbitrarily scaled for graphing purposes, the sizes within each figure are consistent. Figure 26 which plots the energy flow for the non-decomposable 1,3 mode shows most of the acoustic energy propagating through the silicon carbide and leaking into the aluminum. Figure 27 plots the decomposable 0,3 wave. A superimposed longitudinal and shear wave at angles 16° and 59° respectively is represented by the flipping of the ellipses. The resultant wave is also composed of a longitudinal and shear wave, but the longitudinal component is extremely small so the shear component dominates the leakage into the aluminum.

The experimental approach was designed to measure several aspects of the leaky waves. These include leakage angle, wave speed, and a qualitative measure of amplitude. These results from the experimentally measured leaky waves on a silicon carbide/aluminum interface were compared to the general analytical results of Pilant and the theoretical analysis of the silicon carbide/aluminum interface.

VI.3 Experimental Procedures

Specimen Preparation

The requirements of a specimen to study the propagation of leaky waves must have two unique characteristics. First, it must be large enough to allow relatively low frequency ultrasonic waves to propagate while consisting of relevant composite materials. Second, it must have a geometry to allow the angles of leakage to be determined. A silicon carbide/aluminum specimen was chosen because of its widespread use in metal matrix composites and since several leaky modes are believed to exist in these materials. An aluminum hemisphere 4 inches in diameter was machined to enable determination of the leakage angle, since as with all high modulus fiber reinforcement in relatively low modulus matrix composites the leakage is into the metal matrix. Two aluminum shims approximately the same diameter as the transducer face were also machined from the same block of 2024 aluminum to focus the wave and to allow the flat transducer faces to conform to the curvature of the hemisphere. They were attached to the transducers by a solid wax couplant obtained from Acoustic Emission Technology Corporation.

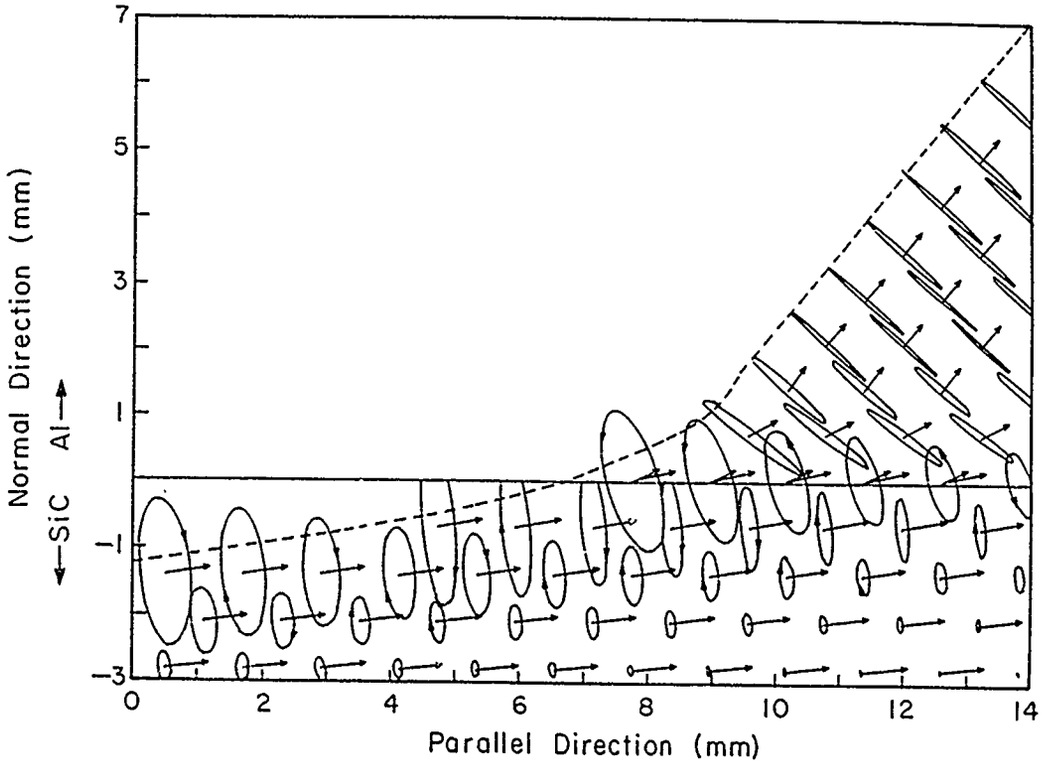

Figure 15. Representation of the displacement field of a non-decomposable leaky wave propagating on a silicon carbide/aluminum interface. The ellipses trace the orbit of a particle and the arrowheads show particle motion. The arrows show the energy flow averaged over one period.

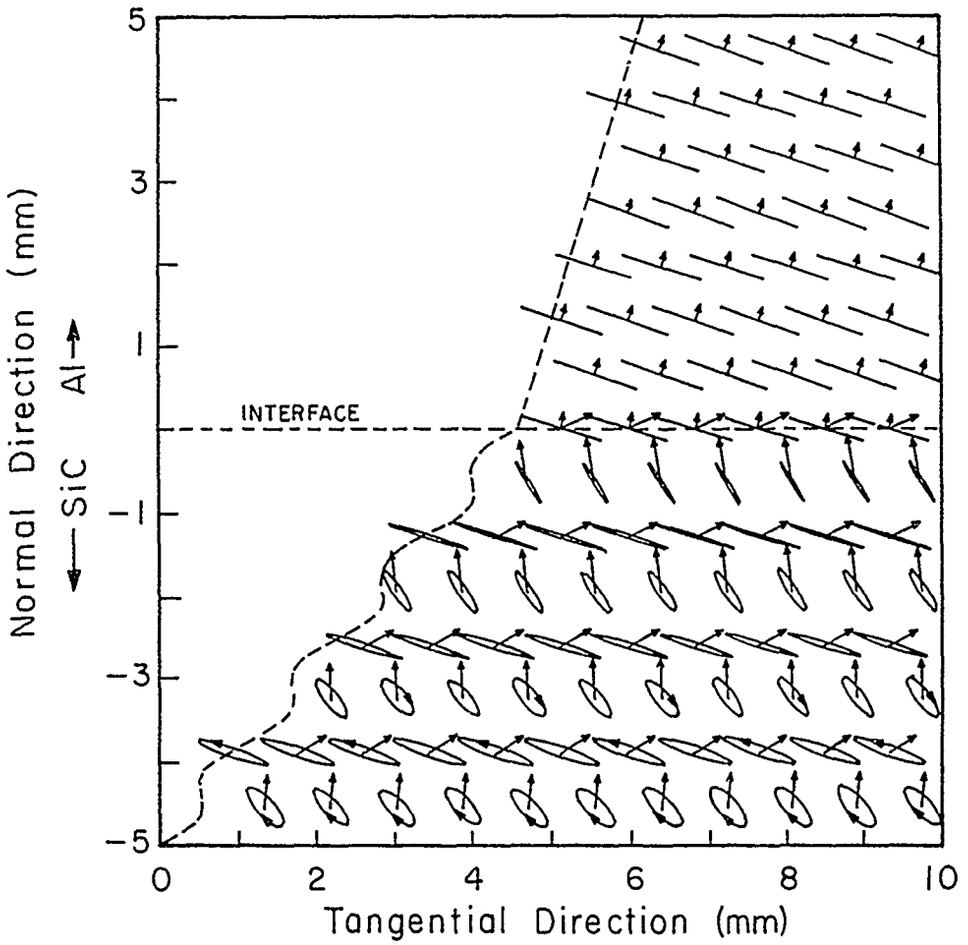

Figure 27. Representation of the displacement field of a decomposable leaky wave propagating on a silicon carbide/aluminum interface. The ellipses trace the orbit of a particle and the arrowheads show particle motion. The arrows show the energy flow averaged over one period.

TABLE XII

Measured Elastic Constants of SiC and 6061 Al						
	r g/cm^3	E GPa	G GPa	B GPa	ν	V_R m/sec
Silicon Carbide	3.1323*	410	180	208	0.16	6831
6061 Aluminum	2.70	66	24	74	0.35	2850

*measured by water displacement technique at Standard Oil Engineering Material Labs

The sintered SiC plate 4" x 4" x 3/4" was obtained from the Standard Oil Engineered Materials Company. Table XII lists the measured physical properties of the silicon carbide and aluminum. The elastic constants were determined by conventional pulse-echo ultrasonic techniques.

VI.4 Experimental Measurement Technique

Leaky waves were generated on the SiC/Al interface through a mode conversion from incident longitudinal waves. Pairs of 1, 5, and 7.5 MHz commercial longitudinal transducers 0.5 inches in diameter were mounted on the aluminum shims with a solid wax couplant. These in turn were coupled to the aluminum hemisphere by silicone grease. Additionally, a pinducer was mounted at the far end of the specimen normal to the SiC/Al interface. The specimen was fixed to a rotation stage which allowed precise determination of the incident and reflected angles. A schematic of the experimental apparatus is shown in Figure 28.

Ultrasonic waves were generated using a conventional pitch-catch technique which utilized a MATEC Pulser Receiver (Model 6600) and a Hewlett Packard A-scan Oscilloscope (Model 1743A). The Δ time mode of the oscilloscope provided two intensified delayed sweeps which could be positioned at any point relative to the main oscilloscope sweep. These were positioned over the main-bang and either the reflected wave or the leakage from an interface wave. To determine velocity, these two signals were expanded to full screen and overlapped utilizing the 100 MHz crystal timing reference to directly measure the time difference between the two signals. The oscilloscope permitted travel time measurements to within one nanosecond.

Longitudinal waves were generated by the transducers in the aluminum shims. This focused wave was introduced into the hemisphere and allowed to reflected off the interface. Detection was accomplished by the second longitudinal transducer mounted on the opposite side of the hemisphere. Silicone grease was used as the couplant between the aluminum shims and the aluminum hemisphere. Simultaneous monitoring of energy propagating along the interface was accomplished by the pinducer. The 1.5 mm diameter pinducers obtained from Valpey-Fisher utilizes a 1 mm thick PZT 5A element. These transducers are nominally 4 MHz and extremely broadbanded. Measurements were conducted with no bonding between the surfaces and with the surfaces joined by epoxy. Travel times were measured at 5 degree increments from zero to 85 degrees with the transducers placed symmetrically about the normal axis of the hemisphere. The receive transducer was also scanned along the side of the hemisphere from its position

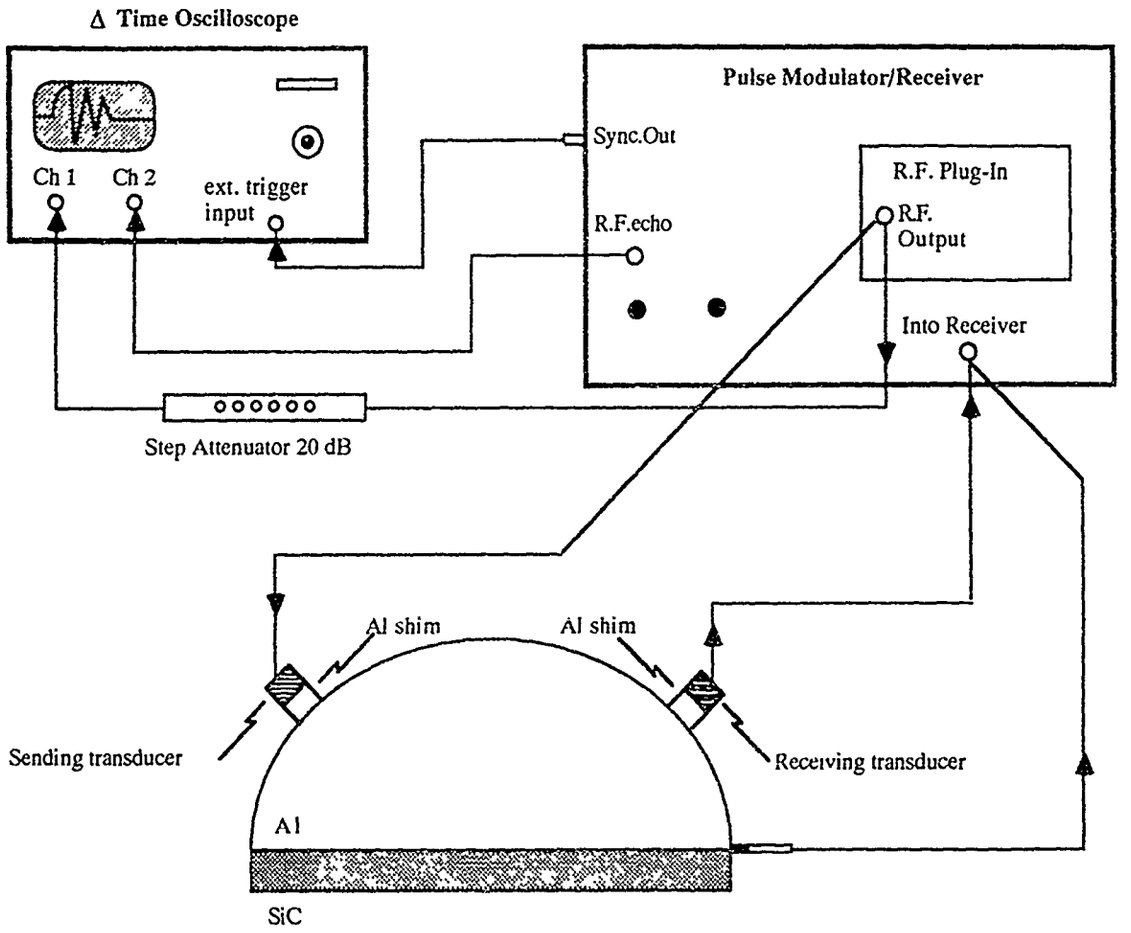

Figure 28. Schematic of the experimental apparatus used to measure the travel times of the leaky waves at a planar silicon carbide/aluminum interface.

to the interface at the predicted angles of leaky wave generation to measure the leaked energy. When an signal was detected by the pinducer, increments of the sending transducer were decreased by 1 degree.

Finally, direct measurement of the leakage energy was made keeping the sending transducer fixed at its position when a signal was detected at the interface by the pinducer. The receive transducer was then moved to allow the pinducer to scan the side of the hemisphere in several degree increments.

VI.5 Results and Discussion

The measured travel times for both the receive transducer and the pinducer in the case of casual contact are shown in Figure 29 for the 5 MHz transducers. Degrees are measured counter-clockwise from the right interface edge arbitrarily designated 0 degrees to the normal at 90 degrees for the received signal. The incident wave degree designation is a mirror reflection of this with the normal also at 90°. The travel times were used to calculate wave velocity by subtracting the travel times through the two shims which was determined by a pulse-echo technique to be 5.053 microseconds. Figure 29 shows that the longitudinal wave incident on the interface was reflected and detected by the receive transducer. The reflected wave traveled with at the longitudinal velocity of approximately 6284 m/sec. No attempt was made to quantitatively measure the reflected bulk wave amplitudes or to evaluate the reflected bulk waves themselves. A review of acoustic pressure values at free boundaries and at solid-liquid boundaries is presented in several manuscripts including Ultrasonic Testing of Materials by Krautkramer [32].

The fact that no energy was measured by the pinducer placed on the interface at any of the incident angles indicated that all of the energy was being reflected or refracted. There was no generation of interface waves at angles between 5° and 85° suggesting that no bonding was apparent to the incident acoustic wave. This case, where the aluminum hemisphere was placed in casual contact with the SiC plate, is representative of a complete lack of bonding as determined acoustically. Results from the 1 and 7.5 MHz waves are identical to the 5 MHz results shown above. At zero applied pressure the ultrasonic wave travels with the velocity of a surface wave. The important condition of existence for a Rayleigh surface wave is a free surface. The fact that an ultrasonic wave propagates with the Rayleigh velocity indicates that it travels on the titanium surface and sees a free surface instead of the steel. This reflects that the acoustic wave senses a complete lack of bonding between the two surfaces. This is

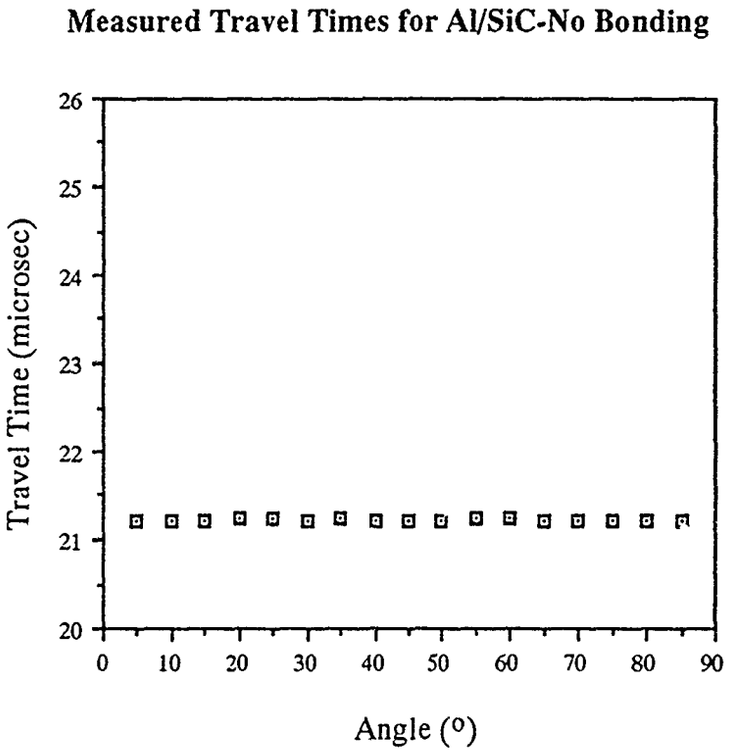

Figure 29. Measured travel times of the 1MHz longitudinal wave reflected by an unbonded silicon carbide plate and an aluminum hemisphere over a range of incident angles. The velocity of this longitudinal wave measured by the receive transducer was 6284 m/sec.

also the case with the silicon carbide/aluminum interface. With the aluminum hemisphere resting on the silicon carbide, the acoustic wave sensed no bonding between the surfaces. No interface wave was detected by the pinducer and no refracted wave was detected in the silicon carbide. This was also confirmed by propagating a Rayleigh wave on the silicon carbide using the Rayleigh wedges shown in Figure 10. The velocity of the Rayleigh wave was determined to be 6831 m/sec. When the aluminum was bonded to the silicon carbide by a thin layer of glue, two distinct leaky modes were evident at 1 MHz. Figure 30 is a plot of the measured travel times for the receive transducer as a function of its transducer position. Superimposed on this plot are the measured travel times of the pinducer as a function of the transmitting transducer position. The pinducer output reflects the appearance of two leaky modes which occur at approximately 23° and at 55°. The transmitting angle was changed to one degree increments as soon as pinducer input was detected. Although no effort was made to quantitatively measure the amplitude of the detected signal at the second transducer, the appearance of the reflected longitudinal wave even at leaky wave angles indicates that only a fraction of the energy is mode converted into a leaky wave. Several factors including beam spread and difficulties determining exact reflection angle made amplitude measurements impractical.

Figure 31 is a schematic representation of both the no bond case and the bonded case. When the two surfaces are in casual contact, the reflected wave is detected by the receive transducer. There is no signal at the interface. However, when the two surfaces are bonded with epoxy, the reflected wave is detected by the receive transducer and the interface wave detected by the pinducer at approximately 23° and 55°.

The measured travel times of the two waves at approximately 23° and 55° represent a combination of velocities which follow a law of mixtures type argument. It is composed of a longitudinal wave which passes through the aluminum shim and then propagates through the aluminum hemisphere a distance equal to the radius of the hemisphere. At the interface, part of this wave is mode converted to a leaky wave which travels the length of the radius at the interface and is detected by the pinducer. By subtracting the initial longitudinal wave from the travel time, leaky wave velocity information was determined. This is shown in Figure 32. The leaky wave generated by mode conversion from approximately 53° to 57° traveled at a velocity of 10064 ± 82 m/sec. The second leaky wave generated from approximately 21° to 25° traveled at a velocity of 5224 ± 119 m/sec.

The velocity of the wave generated by mode conversion at 55°± 2° implies that it is largely affected by the silicon carbide whose longitudinal velocity is 11965 m/sec. As

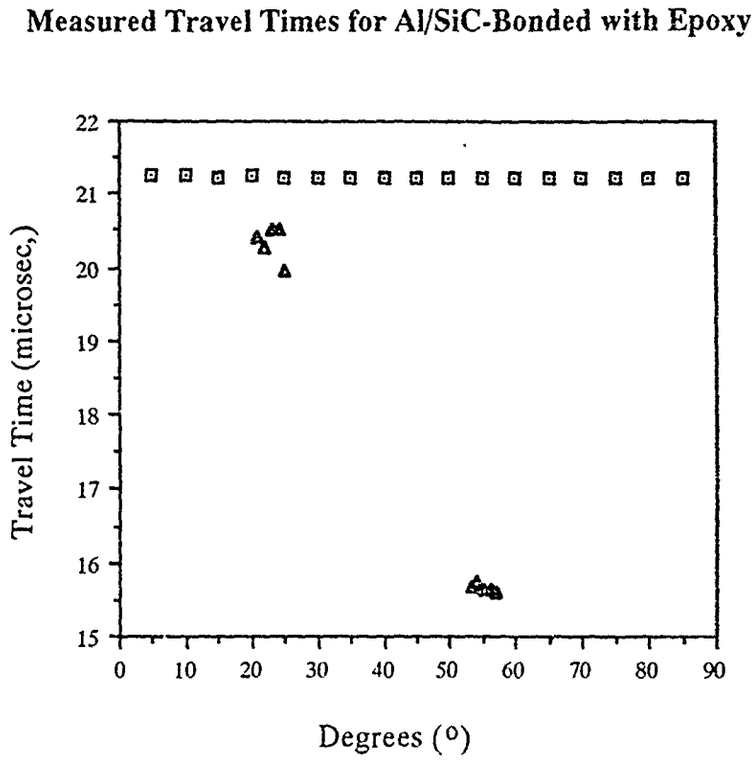

Figure 30. Measured travel times of a 1MHz ultrasonic wave reflected by a silicon carbide plate bonded to an aluminum hemisphere over a range of incident angles. Pinducer output is represented by the triangles and the longitudinal receive transducer output is represented by the squares.

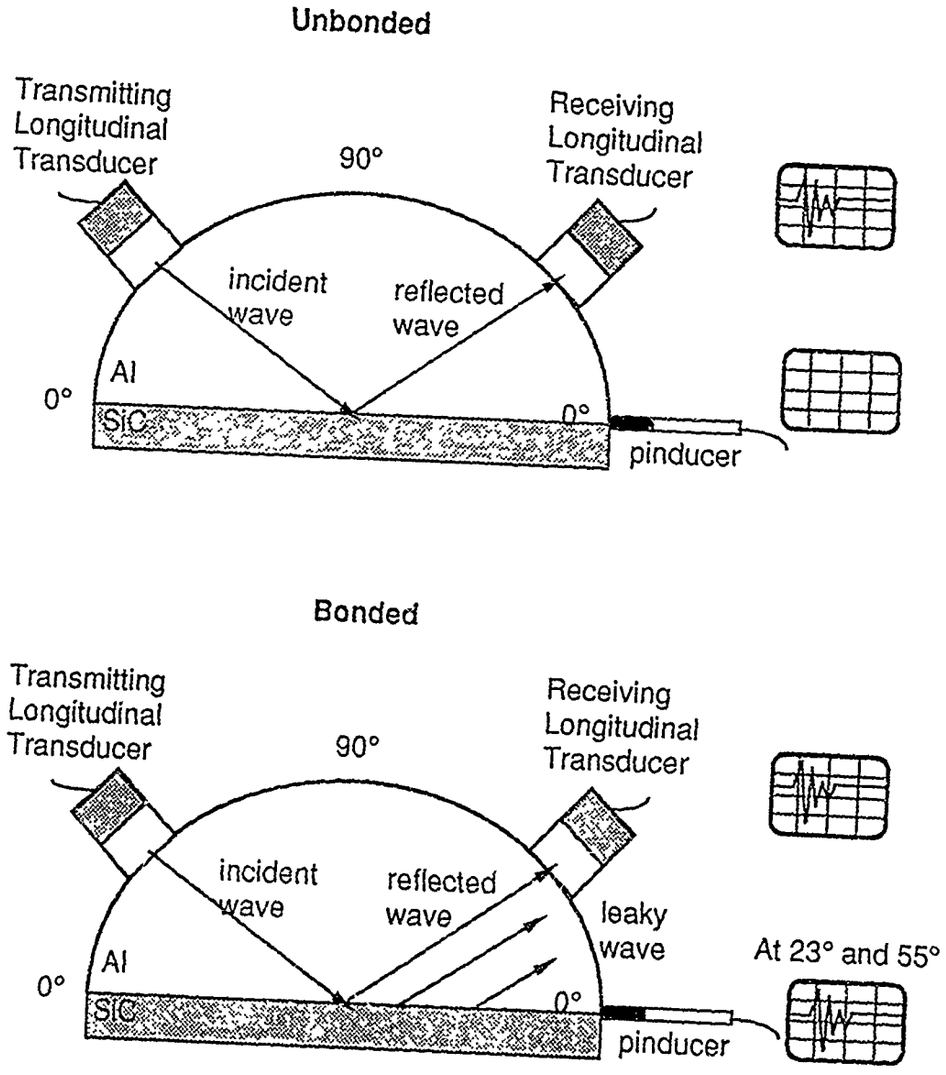

Figure 33. Schematic representation of the wave propagation and transducer output signals for both the bonded and unbonded cases.

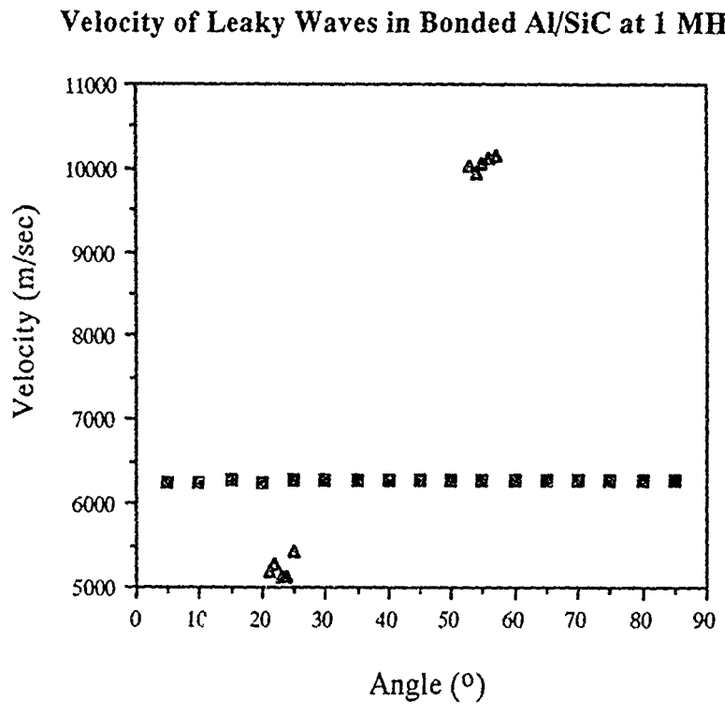

Figure 32. Velocities of the 1 MHz leaky waves generated at a planar silicon carbide/aluminum interface at two incident angles.

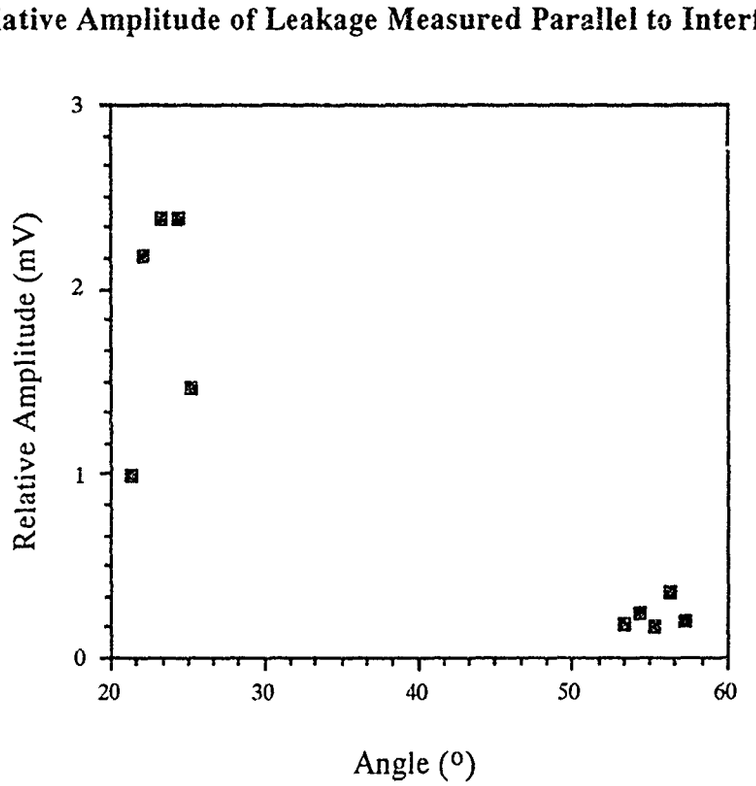

Figure 33. Relative amplitudes of the two leaky waves measured by the pinducer mounted at the interface.

this wave propagates along the interface, an examination of the displacement field normal to the interface would show that the majority of the energy is propagated through the denser silicon carbide as predicted by analytical studies. Energy is leaked away from the interface through the lighter media, aluminum in this case, at a fairly steep angle (~55°) indicating a relatively attenuative leaky wave. The second wave has a much shallower leakage angle approximately 23°± 2° and is less attenuative than the faster wave. This is corroborated by Figure 33 which plots the relative amplitudes of the leaky waves as measured by the pinducer. Since more energy is radiated away from the 55° leaky wave, its relative displacement amplitude measured by the pinducer parallel to the interface is much less than that of the 23° wave. Therefore the steeper leaky wave appears as the more attenuative wave. This leaky wave travels at a much slower velocity of approximately 5224 m/sec. This wave appears to be largely affected by the aluminum, since its leaky wave velocity is closer to that of the longitudinal wave velocity of the aluminum. The leakage is also into the aluminum, but at a much steeper angle.

The appearance of these interface waves also demonstrates the effectiveness of remotely generating leaky waves by mode conversion through the bulk of one of the materials. The critical angles of generation are consistent with the angles of leakage for the these waves so that any modes that exist can be generated by varying the incident angle of the transducer.

These two waves correlate well to the analytically predicted leaky modes in a planar silicon carbide/aluminum interface. The first leaky wave experimentally measured corresponds to the non-decomposable (0,3) leaky mode predicted to leak at an angle of 21.0° and travel with a velocity of 5562 m/sec. The experimentally determined wave had a leakage angle of 23° ± 2° and traveled at a velocity of at 5224 ± 119 m/sec. The (1,3), (2,3), and the (1,1) analytical modes leak at angles of 49.0°, 49.2°, and 48.3° respectively. Although the experimental measurement of the leaky waves was not able to distinguish three individual modes, the fastest mode was observed. The (1,3) mode has a leakage angle of 49.0° and a predicted velocity of 8643 m/sec. This corresponds to the appearance of the second experimentally observed leaky wave at 55°± 2° which travelled with a velocity of 10064 ± 82 m/sec. The three analytical modes are grouped within one degree of each other and therefore could not be distinguished experimentally by leakage angle. Only the fastest of these three modes the (1,3) was detected by the pinducer. Several possible explanations exist to adequately account for this fact. One is that the waves were not generated at all. The incident transducer was increased by increments of one degree, the workable limit of the translators. Although the beam spread of the incident longitudinal wave should have covered all possible angles, it is

conceivable that the bulk of the energy was never directed exactly at the angles needed for mode conversion into the (2,3) or (1,1) analytical leaky modes. However, assuming that the leaky waves were generated, another possibility is that they completely attenuated before reaching the pinducer at the edge of the interface (see Figure 28). If the majority of the energy was leaked away from the interface, the arrival of the leakage at the second transducer would have been masked by the reflecting longitudinal wave whose arrival time is within several nanoseconds of both of these two leaky waves. Additionally, the amplitude of the longitudinal wave would have been much larger than either leaky wave. Consequently, the arrival of the leaky wave at the pinducer would have been undetectably small.

No attempt was made to measure any of the decomposible leaky modes. This was due to the potential difficulty generating these modes and the questionable ability of measuring the generation and leakage angles with any accuracy.

Figures 29 and 30 show the two extreme cases of zero bonding and complete bonding which are measured in terms of the presence of a leaky wave and its velocity. Utilizing these types of measurements, the quality of an interfacial bond may be examined by nondestructive acoustic means. The measurement of an specific interface wave velocity for known propagation distances will allow the bond along that interface to be qualitatively determined. By decomposing the measured interface wave velocity into its leaky wave and/or Rayleigh wave components through a law of mixtures type argument, the contribution of the Rayleigh wave can be determined and directly related to the amount of disbonding. In the same manner, the percentage contribution of the leaky wave can be directly related to the percentage by bonding.

Figure 34 shows the velocities of the leaky waves measured at 5 MHz. One leaky wave appeared between 54° and 60°. The interface wave velocity was measured to be 10020 ± 282 m/sec. This wave is analogous to the one observed at 55° ± 2° at 1 MHz and also to the (1,3) analytical mode. The velocity indicates that the bulk of the energy is propagated through the silicon carbide and that the leakage is into the aluminum. The steeper leakage angle is again representative of a more attenuative interface wave.

Another leaky wave occurred between 24° and 35°. Its velocity was measure to be 5365 ± 394 m/sec. This waves is similar to the one measured at 23° ± 2° at 1 MHz and the (0,3) analytical mode. Its slower velocity indicates that the bulk of its energy is propagated through the aluminum and that the leakage is also into the aluminum hemisphere, but at a much shallower angle. This wave is less attenuative than the leaky wave that appeared at the steeper angle.

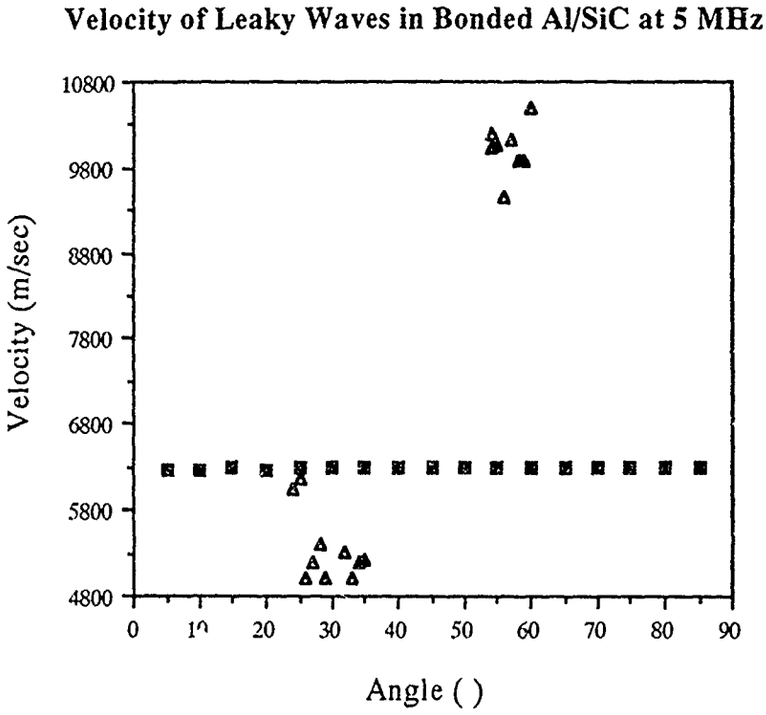

Figure 34. Velocities of the 5 MHz leaky waves generated at a planar silicon carbide/aluminum interface at two incident angles.

No consistent measurements were produced utilizing the 7.5 MHz transducers. Inconsistent travel times and low amplitude measurements were characteristic of the difficulties encountered at this frequency.

It is clear that at these relatively low ultrasonic frequencies that the leaky waves are non-dispersive. The velocities of shallower wave at 1 MHz and 5MHz are 5562 ± 119 m/sec. and 5365 ± 349 m/sec. respectively, within 4 percent of each other while the velocities of the steeper wave are within less than 1 percent of each other. The mean leakage angles of the steeper wave 57° and 55° are within two degrees of each other, however the shallower leakage angles show a slight discrepancy. At 1 MHz the leakage angle is 23° ± 2° and at 5 MHz the leakage angle becomes 29.5° ± 3.5°. Although this variance is too large to be explained by the shift in energy flow (analogous to the Goos-Hanchen shift in optics), its probable cause is the fact that the diameter of the sending and receiving longitudinal transducer faces covers an arc of several degrees when placed on the hemisphere. Care was taken to place both transducers in symmetric positions, however, any slight variation in one of the transducers would cause an error in both angular measurements.

Direct measurement of the leakage at both generation angles was also accomplished. Figure 35 shows the measured relative amplitudes of the leakage of the first interface wave to appear at 1 MHz. At a specific incident angle of generation of leaky waves determined by a pinducer signal at the interface, the pinducer was scanned along the reflected face of the aluminum hemisphere. Figure 35 shows the relative amplitudes of the leakage for an interface generated at an incident angle of 23°. A line drawn from the center of the hemisphere which corresponds to the point of generation of the leaky wave through the maximum leakage point shows the angle of leakage to be consistent with the incident angle. Note that by earlier definition the center of the hemisphere corresponds to the 90° designation at the surface of the hemisphere. This line represents the angle of maximum acoustic energy flow of the leakage away from the interface.

Figure 36 shows the direct leakage measurements of an interface wave generated from an incident angle of 55°. Its relative leakage amplitude maximum is larger than that of the leakage from the 23° wave. This substantiates the contention that the steeper leaky wave is the more attenuative of the two interface waves. The line drawn from the point of generation of the wave on the interface through the maximum leakage points again shows that the angle of maximum energy flow away from the interface is consistent with the incident angle of generation.

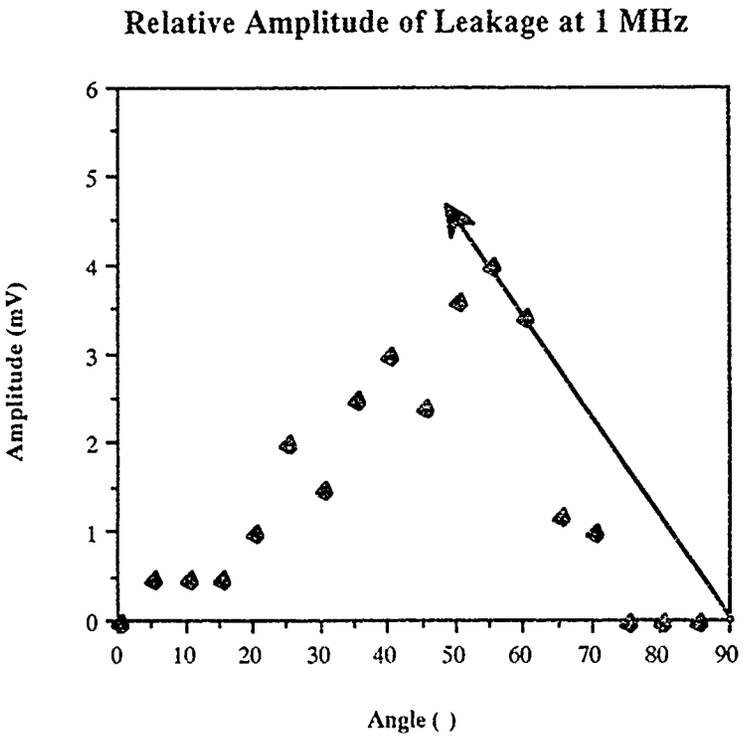

Figure 35. Direct measurement of leakage amplitude for the 1MHz leaky wave generated at ~23 as measured by the pinducer on the aluminum hemisphere surface over a range of angles.

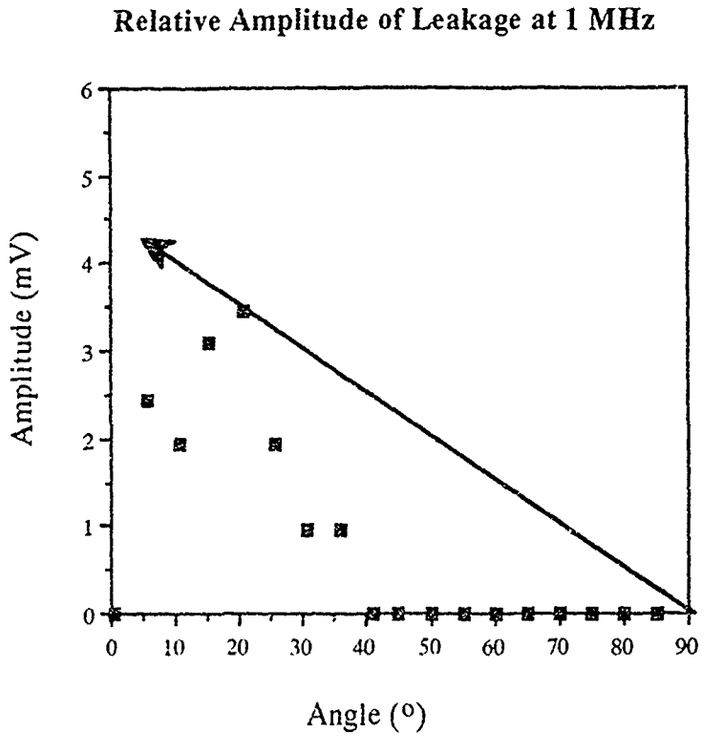

Figure 36. Direct measurement of leakage amplitude for the 1MHz leaky wave generated at ~55° as measured by the pinducer on the aluminum hemisphere surface over a range of angles.

Remote generation and detection of leakage and leaky waves demonstrated by these experiments offers even greater possibilities for nondestructive acoustic evaluation of the interfacial structure. While direct measurement of leaky waves offers several benefits as describe previously, results from figures 33, 34, 35, and 36 allow considerable insight into the structure and properties of the planar silicon carbide/aluminum interface. Each leaky wave propagates through both materials and contains certain information about the elastic properties of the interface depending on the mode. Remote generation by reflection from a surface generated bulk wave allows the potential for all modes to be produced. Additionally, detection of the leakage at the surface of either material is crucial for nondestructive interface characterization. By measuring the leakage or absence of leakage of a certain leaky mode, the presence and location of disbonding can be determined. Leakage measurements also offer insight into the elastic character of both of the materials comprising the interface as well as the interface itself if that structure is different (i.e. heat affected zone, etc.).

VI.6 Conclusions

1. Two leaky modes were remotely generated by mode conversion from a bulk wave incident on a bonded silicon carbide/aluminum interface at a critical angle. One wave was generated at ~23° and travelled with a velocity of ~5224 m/sec, while the second leaky wave was generated at ~55° and travelled with a velocity of 10064 m/sec. It was concluded that remote generation is a valuable method for exciting leaky modes when direct access to the interface is impossible.

2. Theoretical analysis by NIST computer modeling predicts four decomposable modes and six non-decomposable modes for a planar silicon carbide/aluminum interface. Two of these have been experimentally verified.

3. No interface waves were generated on the unbonded silicon carbide plate and the aluminum hemisphere.

4. Relative amplitude measurements of the leakage energy show that maximum leakage energy of the steeper wave was greater than that of the shallower wave. Direct measurement of the leaky wave amplitude at the interface confirmed this fact. It was concluded that the steeper wave was more attenuative than the shallower leaky wave.

5. Measurements utilizing 5 MHz longitudinal transducers produced two leaky waves with leakage angles of approximately 29.5° and 57° with velocities of approximately 5365 m/sec. and 10020 m/sec. respectively. These measurements did not reveal any significant advantages or disadvantages of using a s''ghtly higher frequency for generation of interface waves. The slight shift in leakage angle was probably due to the fact that the incident transducer face covered an arc of about 5° on the aluminum hemisphere and resulted in slightly shifted angular measurements.

6. Remote measurement at the surface of the aluminum hemisphere of the leakage energy was accomplished. These measurements confirmed that the leakage angle was the same as the incident generation angle. It was concluded that this direct measurement of leakage is a valuable method for separating modes and will contribute to nondestructive interface characterization.

7. It was shown that leaky waves offer several potential benefits for nondestructive interface wave characterization including detection of disbonds and elastic characterization.

VII. References

1. Stoneley, R., Proc. Roy Soc., *106*, p.416 (1924).

2. Rayeligh, Lord, Proc. Lond. math. Soc., *17*, 4 (1885).

3. Love, A.E.H., A Treatise on the Mathematical Theory of Elasticity. New York, Dover, (1944).

4. Viktorov, I.A., Rayleigh and Lamb Waves. New York, Plenum, (1967).

5. Sezawa, K., Kanai, K., Bull. Earthquake Res. Inst., *17*, p.1 (1939).

6. Sezawa, K., Kanai, K., Bull. Earthquake Res. Inst., *16*, p.683 (1938).

7. Sezawa, K., Kanai, K., Bull. Earthquake Res. Inst., *16*, p.504 (1938).

8. Scholte, J.G., R. Astron. Soc. London Monthly Notices Geophys. Suppl., *5*, p.120 (1947).

9. Scholte,J.G., Proc. Ned. Akad. V. Wetensch. Amst., *45*, pp. 20, 159 (1942).

10. Yamaguchi, R., Sato, Y., Bull. Res. Earthquake Inst., *33*, p.549 (1955).

11. Ginzbarg, A.S., Strick, E., Bull. Seismol. Soc. Am., *48*, p.51 (1958).

12. Owen, T.E., Prog. Appl. Mater. Res., *6*, p.69 (1964).

13. Lim, T.C., Musgrave, M.J.P., Nature, *225*, p. 372 (1970).

14. Chadwick, P., Currie, P.K., Quart. J.Mech. Appl. Math., *27*, p.497 (1974).

15. Pilant, W.L., Bull. Seismol. Soc. Am., *62*, p.285 (1975).

16. Lee, D.A., Corbly, D.M., IEEE Trans Sonics Ultrason., *SU-24*, p.206 (1977).

17. Claus, R.O., Palmer, C.H., IEEE Trans Sonics Ultrason., *SU-27*, p.97 (1980).

18. Claus, R.O., Palmer, C.H., Appl. Phys. Lett., *31*, p.577 (1977).

19. Claus, R.O., Proc. SPIE, *192* (1979).

20. Claus, R.O., Kline, R.A., J. Appl. Phys., *50*, July, p.8066 (1979).

21. United States Steel, Isothermal Transformation Diagrams, United States Steel Publ., p.109, 1964.

22. Schoonover, R.M., Davis, R.S., Procedings of the 8th Conference of the IMEKO, Poland, 1980.

23. Davis, R.S., Metrologia, *18,* p. 193, 1982.

24. Elkind, B.J., "Ultrasonic Characterization of microstructurally modified Surfaces of Steel Subjected to Electron Beam Irradiation", Master's Thesis, 1984.

25. Dieter, G.E., Mechanical Metallurgy, New York: McGrawHill Inc., 1975.

26. United States Steel, Isothermal Transformation Diagrams, United States Steel Publ., p.105, 1964.

27. American Society for Metals, Metals Handbook, Vol. 3, ASM Publ., p. 388, 1980.

28. Elkind, B.J., "Ultrasonic Characterization of Microstructurally Modified Surfaces of Steel Subjected to Electron Beam Irradiation", Master's Thesis, 1984.

29. Bethlehem Steel Company, Modern Steels And Their Properties, p. 124, 1961.

30. Estermann, T., Complex Numbers and Functions, London, Athlone Press (1962).

31. Krasicka, E., Simmons, J., Propagation and Dispersion of Radial-Axial Leaky Modes in Infinitely Clad Rods., to be published.

32. Krautkramer, J.,Krautkramer, H., Ultrasonic Testing of Materials. Berlin, Heidelberg, and New York, Springer, 1977.